



저작자표시-비영리-변경금지 2.0 대한민국

이용자는 아래의 조건을 따르는 경우에 한하여 자유롭게

- 이 저작물을 복제, 배포, 전송, 전시, 공연 및 방송할 수 있습니다.

다음과 같은 조건을 따라야 합니다:



저작자표시. 귀하는 원저작자를 표시하여야 합니다.



비영리. 귀하는 이 저작물을 영리 목적으로 이용할 수 없습니다.



변경금지. 귀하는 이 저작물을 개작, 변형 또는 가공할 수 없습니다.

- 귀하는, 이 저작물의 재이용이나 배포의 경우, 이 저작물에 적용된 이용허락조건을 명확하게 나타내어야 합니다.
- 저작권자로부터 별도의 허가를 받으면 이러한 조건들은 적용되지 않습니다.

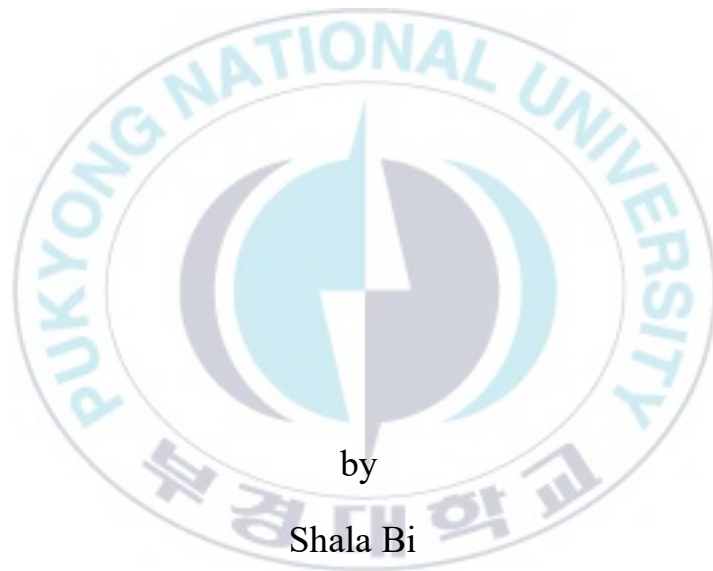
저작권법에 따른 이용자의 권리는 위의 내용에 의하여 영향을 받지 않습니다.

이것은 [이용허락규약\(Legal Code\)](#)을 이해하기 쉽게 요약한 것입니다.

[Disclaimer](#)

Thesis for the Degree of Doctor of Philosophy

Luminescence Properties of Eu^{3+} and Mn^{2+} Doped Tungstate and Phosphate Materials



by

Shala Bi

Department of Physics

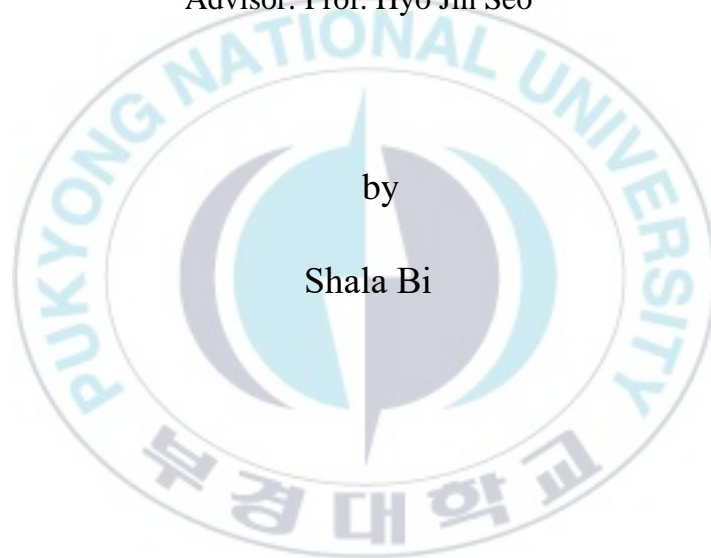
The Graduate School

Pukyong National University

August 2022

**Luminescence Properties of Eu^{3+} and Mn^{2+}
Doped Tungstate and Phosphate Materials**
(Eu^{3+} 와 Mn^{2+} 이온이 도핑된 텅스텐산염
및 인산염 물질의 형광 특성)

Advisor: Prof. Hyo Jin Seo



A thesis submitted in partial fulfillment of the requirements for the
degree of
Doctor of Philosophy

in Department of Physics The Graduate School,
Pukyong National University

August 2022

Luminescence Properties of Eu^{3+} and Mn^{2+} Doped Tungstate and Phosphate Materials

A dissertation

by
Shala Bi

Approved by:

(Chairman: Prof. Cheol Woo Park)

(Member: Prof. Jae Heung Koo)

(Member: Dr. Kyoung Hyuk Jang)

(Member: Prof. Jae Yong Je)

(Member: Prof. Hyo Jin Seo)

August 26th, 2022

CONTENTS

List of Figures	iii
List of Table	v
Abstract	vi
1. Introduction.....	1
1.1 Introduction of luminescent materials.....	1
1.1.1 Definition and classification of luminescence.....	1
1.1.2 Composition of luminescent materials.....	3
1.2 Rare earth luminescence	4
1.2.1 Rare earth ions	4
1.2.2 Electronic configuration of rare earth elements	5
1.2.3 The unique spectroscopic characteristics of rare earth ions	7
1.2.4 4f-4f transitions	8
1.2.5 4f-5d transitions	9
1.2.5 Luminescence of Eu^{3+} ions	10
1.3 Transition metal Mn ion luminescence	12
1.3.1 Luminescence of Mn^{2+}	12
1.4 Energy transfer.....	13
1.5 Implementation of white light diodes	14
1.6 Scopes of this thesis	16
2. Experimental and Characterization	16
2.1 Sample preparation	16
2.1.1 Synthesis of $\text{Ca}_3\text{WO}_5\text{Cl}_2$ and Eu^{3+} doped $\text{Ca}_3\text{WO}_5\text{Cl}_2$	16
2.1.2 Synthesis of $\text{Na}_2\text{Mg}_{1-x}(\text{PO}_3)_4:x\text{Mn}^{2+}$ ($x=0.01, 0.03, 0.05, 0.07, 0.09, 0.11$)	17
2.2 Material Characterization.....	18
2.2.1 X-ray Diffraction.....	18
2.2.2 Scanning Electron Microscopy	19
2.2.3 Photoluminescence Emission and Excitation Spectroscopy	19
2.2.4 Fluorescence Decay Time	21
2.2.5 Temperature dependent photoluminescence.....	21
2.2.6 Color Coordinate.....	22
2.2.7 Thermal stability activation energy	23
3. Synthesis, crystal structure and luminescent properties of Eu^{3+} -activated halotungstates applied in W-LEDs	24
3.1 Introduction.....	24
3.2 Results.....	25
3.2.1 Structural and properties of pure $\text{Ca}_3\text{WO}_5\text{Cl}_2$	25
3.2.2 Self-activated luminescence of the $\text{Ca}_3\text{WO}_5\text{Cl}_2$	27
3.2.3 Luminescent performance of $\text{Ca}_3\text{WO}_5\text{Cl}_2:\text{Eu}^{3+}$	32
3.2.4 High-temperature luminescence of $\text{Ca}_3\text{WO}_5\text{Cl}_2:\text{Eu}^{3+}$	40
3.3 Conclusion	43
4. Photoluminescence properties of red-emitting Mn^{2+} -activated $\text{Na}_2\text{Mg}(\text{PO}_3)_4$ phosphors for white-LEDs	44

4.1 Introduction.....	44
4.2 Results.....	45
4.2.1 Crystal structural refinement.....	45
4.2.2 Optical performances	46
4.2.3 Concentration-dependent luminescence properties of Mn ²⁺ -doped Na ₂ Mg(PO ₃) ₄	48
4.2.4 The temperature dependent luminescence properties in Mn ²⁺ -doped Na ₂ Mg(PO ₃) ₄	52
4.3 Conclusions.....	57
References.....	59
Acknowledgements.....	65



List of Figures

Figure 1.1 A luminescent ion A in its host lattice.	3
Figure 1.2 Energy transfer from a sensitiser S to an actixator A..	3
Figure 1.3 The main physical process of luminescence, M: matrix; S: sensitizer; A: activator. 4	
Figure 1.4 The energy transfer from sensitizer to activator, S: ground state of sensitizer; S*: excited state of sensitizer; A: ground state of activator; A1*, A2*: excited state of activator	4
Figure 1.5 The schematic diagram of energy level transition in Eu^{3+} ion.	11
Figure 1.6 (a)(b) The emission spectrum of Eu^{3+} in NaLuO_2 and NaGdO_2	12
Figure 1.7 The Tanabe- Sugano energy diagram of Mn^{2+}	13
Figure 1.8 Three methods of generating white light. (a) red + green + blue-LEDs; (b) UV-LED + RGB phosphors; (c) blue-LED + yellow phosphor.	15
Figure 2.1 The preparation process of the high-temperature solid-state method	17
Figure 2.2 Schematic diagram of Braggs Law.	18
Figure 2.3 Measurement schematic of excitation spectrum	20
Figure 2.4 Measurement schematic of emission spectrum.....	20
Figure 2.5 This CIE gamut chart shows the x,y chromaticity coordinates and color temperature locus. The triangular area covers the gamut of colors defined by standard green, red, and blue colors.33 Figure 2.1 The preparation process of the high-temperature solid-state method	23
Figure 3.1 Experimental (black point) and calculated XRD patterns (red solid line) and their differences (blue solid line) for the Rietveld fit of the $\text{Ca}_3\text{WO}_5\text{Cl}_2$ phosphor. The short vertical lines (pink line) show the position of Bragg reflections of the calculated patterns	26
Figure 3.2 The configuration of the atoms in crystal structures $\text{Ca}_3\text{WO}_5\text{Cl}_2$	26
Figure 3.3 (a) The room temperature PLE and PL spectra of host ($\text{Ca}_3\text{WO}_5\text{Cl}_2$ phosphor) (λ_{em} =560 nm and λ_{ex} =266 nm), and (b) the decay curves of host ($\text{Ca}_3\text{WO}_5\text{Cl}_2$ phosphor) (λ_{em} =704 nm; λ_{ex} = 344 nm)	27
Figure 3.4 (a) Temperature-dependent emission spectra of pure $\text{Ca}_3\text{WO}_5\text{Cl}_2$. (b) Temperature- dependent decay curves of pure $\text{Ca}_3\text{WO}_5\text{Cl}_2$. (c) Calculated lifetime of pure $\text{Ca}_3\text{WO}_5\text{Cl}_2$. (d) Three-level energy scheme.39 Figure 2.1 The preparation process of the high- temperature solid-state method.....	30
Figure 3.5 XRD patterns of $\text{Ca}_3\text{WO}_5\text{Cl}_2:\text{Eu}^{3+}$ phosphors with different Eu^{3+} doping concentration along with the ICSD card (ICSD-2335).....	32
Figure 3.6 SEM images of 3 mol% Eu^{3+} ions doped $\text{Ca}_3\text{WO}_5\text{Cl}_2$ phosphors.....	33
Figure 3.7 The room temperature excitation spectra of $\text{Ca}_3\text{WO}_5\text{Cl}_2:\text{xEu}^{3+}$ (x = 0.1, 1.0, 3.0, 5.0, 7.0 and 9.0 %) phosphors	34
Figure 3.8 (a)The room temperature concentration-dependent emission spectra of $\text{Ca}_3\text{WO}_5\text{Cl}_2:\text{xEu}^{3+}$ (x = 0.1, 1.0, 3.0, 5.0, 7.0 and 9.0 %). (b) Relative intensity of Eu^{3+} . (c) energy transfer efficiency η_T with different doping concentration (d) the plots of I_{S0}/I_S vs $C^{n/3}$	37
Figure 3.9 The schematic view of the coordination geometries around the Eu1 (a), Eu2 (a) and	

Eu ³⁺ (a) polyhedrons.	37
Figure 3.10 The decay curves of the Ca ₃ WO ₅ Cl ₂ :Eu ³⁺ phosphors with different Eu ³⁺ doping concentration	38
Figure 3.11 The CIE and led chips of Ca ₃ WO ₅ Cl ₂ phosphors.....	39
Figure 3.12 Schematic energy level diagram for transfer process between WO ₅ Cl group and Eu ³⁺ ions in Ca ₃ WO ₅ Cl ₂ phosphors	39
Figure 3.13 (a) The temperature dependent emission spectra of Ca ₃ WO ₅ Cl ₂ :Eu ³⁺ (5 mol%) phosphors. (b) The relationship of ln[(I ₀ /I) - 1] vs. 1/kT activation energy graph for thermal quenching of the Ca ₃ WO ₅ Cl ₂ :Eu ³⁺ (5 mol%) phosphors. (c) The temperature dependent decay curves of Ca ₃ WO ₅ Cl ₂ :Eu ³⁺ (5 mol%) phosphors. (d) The calculated lifetime of Ca ₃ WO ₅ Cl ₂ :Eu ³⁺ (5 mol%) phosphors with increasing temperature.....	42
Figure 4.1 XRD patterns of Na ₂ Mg _{1-x} (PO ₃) ₄ :xMn ²⁺ phosphors with different Mn ²⁺ doping concentration sintered at 850 °C for 6 h, along with the standard PDF card (PDF#22-0477).	45
Figure 4.2 (a) The energy-level diagram of Mn ²⁺ ions, (b) PL and PLE spectra of the typical Mn ²⁺ ions doped in Na ₂ Mg(PO ₃) ₄ lattice.....	46
Figure 4.3 a) Luminescence emission spectra (λ _{ex} = 355 nm) of phosphors Na ₂ Mg _{1-x} (PO ₃) ₄ :xMn ²⁺ with different Mn ²⁺ doping concentration. (b) The integrated PL intensity versus the concentration of Mn ²⁺ ions; insert shows the Log(I/x) dependent on Log(x). (c) Luminescence excitation spectra (λ _{em} = 613 nm) of phosphors Na ₂ Mg _{1-x} (PO ₃) ₄ :xMn ²⁺ with different Mn ²⁺ doping concentration. (d) The decay curves (λ _{ex} = 355 nm) of phosphors Na ₂ Mg _{1-x} (PO ₃) ₄ :xMn ²⁺ with different Mn ²⁺ doping concentration.....	52
Figure 4.4 (a) Temperature-dependent emission spectra (λ _{ex} = 355 nm) of phosphors Na ₂ Mg _{0.91} Mn _{0.09} (PO ₃) ₄ . (b) Temperature-dependent luminescence wavelength center and integrated luminescence intensities. (c) The variation in FWHM values from 10-500 K for Na ₂ Mg _{0.91} Mn _{0.09} (PO ₃) ₄ phosphor	54
Figure 4.5 The schematic diagram of CC model used to explain the various intra-d-transition phenomena.....	55
Figure 4.6 Temperature-dependent decay curves (λ _{ex} = 355 nm) of phosphors Na ₂ Mg _{0.91} Mn _{0.09} (PO ₃) ₄ monitored by 613 nm. Insert shows the calculated temperature-dependent luminescence lifetimes of the Mn ²⁺ ions in Na ₂ Mg _{0.91} Mn _{0.09} (PO ₃) ₄ lattice....	56

List of Table

Table 1.1 The electron shell structure and radius of rare earth atoms	6
Table 3.1 the refined crystal parameters of $\text{Ca}_3\text{WO}_5\text{Cl}_2$ and compared with the standard data.	26
Table 3.2 Decay times of $\text{Ca}_3\text{WO}_5\text{Cl}_2$ and some fitting parameters of some luminescent tungstate compounds.....	28
Table 3.3 The doping concentration of Eu^{3+} ions dependent CIE values of $\text{Ca}_3\text{WO}_5\text{Cl}_2:\text{Eu}^{3+}$	32
Table 3.4 The temperature dependent CIE values of $\text{Ca}_3\text{WO}_5\text{Cl}_2:5\text{mol}\%\text{Eu}^{3+}$	43



Luminescence Properties of Eu^{3+} and Mn^{2+} Doped Tungstate and Phosphate Materials

Shala Bi

Physic department, The Graduate School,
Pukyong National University

Abstract

As a new generation of display and lighting source, white LED has the characteristics of high efficiency, energy-saving, green environmental protection, no pollution, sturdiness, long life, fast switching, and easy maintenance. It is one of the most promising high-tech fields in the world in recent years. Combining phosphors with ultraviolet, near ultraviolet or blue light chips is one of the important ways to realize white LEDs. As a key and technically important component of white LEDs, phosphors are of great significance in improving and improving the luminous efficiency, color rendering index, service life and other technical indicators of white LEDs. Therefore, it is necessary to continuously explore and develop new and efficient phosphor material.

Rare earth luminescent materials have a widely applied in the fields of light-conversion luminescent materials such as energy-saving lighting, medical imaging, modern information technology and display detection, and phosphor luminescent materials with high efficiency, stability and good luminescent properties are also used in white LEDs and other applications. significance. Tungstate host materials are often selected as valuable luminescent materials due to their good chemical stability, high luminescence intensity, self-luminescence, and easy preparation. Therefore, the self-activated tungstate matrix and Eu^{3+} -doped tungstate matrix materials have extensive research and application significance. In this study, Eu^{3+} ions doped $\text{Ca}_3\text{WO}_5\text{Cl}_2$ was prepared by the facile high temperature solid-state reaction. The PL-PLE spectra, crystal structure, temperature-dependent luminescence, and decay lifetimes were investigated. Under the excitation of UV light, the pure $\text{Ca}_3\text{WO}_5\text{Cl}_2$ emitted the typical self-activated luminescence from the charge transfer (CT) transitions in $[\text{WO}_5\text{Cl}]^{5-}$ groups. With the increasing temperature from room temperature to 480 K,

the emission intensity decreases, and the emission band shifts to blue. Such reduction due to thermal quenching wherein emission centers are thermally activated through the crossing point between the ground and the excited levels. The concentration dependent emission spectra of $\text{Ca}_3\text{WO}_5\text{Cl}_2:\text{Eu}^{3+}$ shows the characteristic emission peaks of Eu^{3+} ions can be observed in the red emission region at around 615 nm both with the host emission band in the blue emission region at around 450 nm. Accordingly, the band at 450 nm originates from charge transfer behavior of WO_5Cl group, while the sharp lines at 615 nm originates from the ${}^5\text{D}_0\text{-}{}^7\text{F}_2$ transitions of Eu^{3+} ions. As the Eu^{3+} concentration increases, the luminescence intensity of the Eu^{3+} ions increase, while that of the WO_5Cl group band decreases rapidly. The temperature dependent emission spectra indicate $\text{Ca}_3\text{WO}_5\text{Cl}_2:\text{Eu}^{3+}$ phosphor has good thermal stability. Therefore, the results indicate the possibility of present phosphor for Near UV (394 nm excitation), blue LED (450 nm excitation) applications in white light diodes with high thermal stability.

Phosphate system phosphor is an important traditional light-emitting material. Phosphate matrix has good physical and chemical stability, low synthesis temperature, low production cost, complex structure, and can strongly absorb ultraviolet light to achieve high-efficiency emission in the visible spectrum, and widely used. In this study, the traditional high-temperature solid-state reaction method was used to synthesize Mn^{2+} -doped $\text{Na}_2\text{Mg}(\text{PO}_3)_4$ phosphors. The structure was conducted on the basis of X-ray diffraction (XRD), the photoluminescence excitation (PLE) and emission (PL) spectra reveal that the $\text{Na}_2\text{Mg}(\text{PO}_3)_4:\text{Mn}^{2+}$ red phosphor could be excited by ultraviolet (UV) to blue light from 300 to 500 nm, and shows a broadband emission in the spectral region from 550 to 750 nm. The optimum doping concentration of Mn^{2+} ions in $\text{Na}_2\text{Mg}(\text{PO}_3)_4$ lattice was measured to be 9 mol% based on the concentration-dependent PL spectra. To deeply study the thermal stability of $\text{Na}_2\text{Mg}(\text{PO}_3)_4:\text{Mn}^{2+}$ red phosphor, temperature dependent PL spectra and decay curves were measured at various temperature ranging from 10 to 500 K. It is demonstrated that $\text{Na}_2\text{Mg}(\text{PO}_3)_4:\text{Mn}^{2+}$ red phosphors can be simulated as potential materials to produce high-efficiency white-light.

Eu³⁺ 와 Mn²⁺ 이온이 도핑된 텅스텐산염 및 인산염 물질의 형광 특성

Shala Bi

부경대학교 대학원 물리학과

요 약

차세대 디스플레이 및 광원으로서는 백색 LED 는 고효율, 에너지 절약, 녹색 환경 보호, 무공해, 견고성, 긴 수명, 빠른 스위칭 및 쉬운 유지 보수 등의 특성을 가지고 있습니다. 최근 몇 년 동안 세계에서 가장 유망한 첨단 기술 분야 중 하나입니다. 형광체를 자외선, 근자외선 또는 청색광 칩과 결합하는 것은 백색 LED 를 구현하는 중요한 방법 중 하나입니다. 백색 LED 의 핵심적이고 기술적으로 중요한 구성 요소로서 형광체는 백색 LED 의 발광 효율, 연색 지수, 수명 및 기타 기술 지표를 개선하고 개선하는 데 매우 중요합니다. 따라서 새롭고 효율적인 형광체 재료를 지속적으로 탐색하고 개발하는 것이 필요합니다.

희토류 발광 재료는 에너지 절약 조명, 의료 영상, 현대 정보 기술 및 디스플레이 감지와 같은 광 변환 발광 재료 분야에서 광범위한 응용 분야를 가지고 있으며 고효율, 안정성 및 우수한 발광 특성을 가진 형광체 발광 재료는 백색 LED 및 기타 응용 분야에도 사용됩니다. 중요성. 텅스텐산염 호스트 재료는 화학적 안정성이 좋고 발광 강도가 높으며 자체 발광 및 준비가 용이하기 때문에 귀중한 발광 재료로 선택되는 경우가 많습니다. 따라서 자체 활성화 텅스텐산염 매트릭스와 Eu³⁺가 도핑된 텅스텐산염 매트릭스 물질은 광범위한 연구 및 응용 분야에서 의미가 있습니다. 이 연구에서 Ca₃WO₅Cl₂ 도핑된 Eu³⁺ 이온은 손쉬운 고체 상태 반응을 통해 준비되었습니다. PL-PLE 스펙트럼, 결정 구조, 온도 의존 발광 및 붕괴 수명을 조사했습니다. UV 광의 여기에서 순수한 Ca₃WO₅Cl₂는 [WO₅Cl]⁵⁻ 그룹의 전하 이동 (CT) 전이에서 일반적인 자체 활성화 발광을 보여줍니다. 온도가 10K 에서 480K 로 증가함에 따라 방출 강도가 감소하고 방출 대역이 파란색으로 이동합니다. 방출 중심이 지면과 여기 레벨 사이의 교차점을 통해 열적으로 활성화되는 열 담금질로 인한 이러한 감소. Ca₃WO₅Cl₂: Eu³⁺의 농도 의존 발광 스펙트럼은 Eu³⁺ 이온의 특징적인 발광 피크가 약 615 nm 의 적색 발광 영역에서 관찰될 수 있음을 보여주고, 약 450 nm 의 청색 발광 영역의 호스트 발광 대역과 함께 관찰될 수 있다. 따라서 450 nm 의 밴드는 WO₅Cl 그룹의 전하 이동 거동에서 비롯된 반면 615 nm 의 날카로운 선은 Eu³⁺ 이온의 ⁵D₀-⁷F₂ 전이에서 비롯됩니다. Eu³⁺ 농도가 증가함에 따라 Eu³⁺ 이온의 발광 강도는 증가하는 반면 WO₅Cl

그림 밴드의 발광 강도는 급격히 감소한다. 전체 온도 범위에서 최대 방출 파장은 온도에 대한 선형 의존성을 나타냅니다. 결과적으로 온도 의존적 특성은 발광 온도 측정에서 잠재적인 이점이 있습니다. 온도 의존적 방출 스펙트럼은 $\text{Ca}_3\text{WO}_5\text{Cl}_2:\text{Eu}^{3+}$ 형광체가 좋은 열 안정성을 가지고 있음을 나타냅니다. 따라서 결과는 열 안정성이 높은 백색광 다이오드에서 근자외선 (394nm 여기), 청색 LED (450nm 여기) 응용 분야에 형광체가 존재할 가능성을 나타냅니다.

인산염계 형광체는 중요한 전통적인 발광 재료입니다. 인산염 매트릭스는 물리적 및 화학적 안정성이 좋고 합성 온도가 낮고 생산 비용이 낮고 복잡한 구조를 가지고 있으며 자외선을 강력하게 흡수하여 가시 스펙트럼에서 고효율 방출을 달성하고 널리 사용됩니다. 본 연구에서는 Mn^{2+} 이온이 도핑된 $\text{Na}_2\text{Mg}(\text{PO}_3)_4$ 형광체를 합성하기 위해 전통적인 고온 고체 상태 반응 방법을 사용하였다. 구조는 X 선 회절 (XRD), 광발광 여기 (PLE) 및 방출 (PL) 스펙트럼을 기반으로 수행되었으며 $\text{Na}_2\text{Mg}(\text{PO}_3)_4:\text{Mn}^{2+}$ 적색 형광체가 자외선 (UV) 에서 청색으로 여기될 수 있음을 보여줍니다. 300 ~ 500 nm 의 빛을 방출하고 550 ~ 750 nm 의 스펙트럼 영역에서 광대역 방출을 보여줍니다. $\text{Na}_2\text{Mg}(\text{PO}_3)_4$ 격자에서 Mn^{2+} 이온의 최적 도핑 농도는 농도 의존적 PL 스펙트럼을 기반으로 9 mol%로 측정되었습니다. $\text{Na}_2\text{Mg}(\text{PO}_3)_4:\text{Mn}^{2+}$ 적색 형광체의 열 안정성을 심층적으로 연구하기 위해 10~500K 범위의 다양한 온도에서 온도 의존성 PL 스펙트럼 및 붕괴 곡선을 측정했습니다. $\text{Na}_2\text{Mg}(\text{PO}_3)_4:\text{Mn}^{2+}$ 적색 형광체는 고효율 백색광을 생성하기 위한 잠재적인 재료로 시뮬레이션됩니다.

1. Introduction

1.1 Introduction of luminescent materials

1.1.1 Definition and classification of luminescence

Luminescent substances are substances that can absorb external energy (mainly radiant energy, chemical energy, electrical energy, etc.) and convert it into optical radiation. Generally, the total energy of optical radiation emitted by luminescent substances is lower than the total energy absorbed. Another part of the energy will be dissipated in the form of thermal radiation. Luminescent substances, as the name implies, are substances with luminescence phenomena, and the light radiation they emit is usually located in the visible light region. Luminescent substances do not always have practical application value [1, 2].

The most fundamental difference between solid-state luminescence and other luminescence is that solid-state luminescence has a longer duration. That is, when the excitation stops, the light-emitting process does not disappear immediately, but gradually weakens until finally disappears. This process is also called the "afterglow" phenomenon. The long duration can reach more than ten hours, and the short duration can also be 10^{-10} s. In this way, according to the duration of the luminescence, the luminescence can be divided into two categories: the duration of less than 10^{-8} s is called fluorescence, and the duration of more than 10^{-8} s is called phosphorescence [3-5].

In the actual research and application process, solid-state luminescence is often divided into the following categories according to the different excitation sources:

1. Photoluminescence: Refers to the object irradiated by external light sources to absorb energy, and through the process of energy transfer and emission, the light is finally formed. To achieve different luminescence purposes and produce different luminescence results, ultraviolet light, visible light, or infrared light is often selected as the excitation light source according to needs, and photoluminescence is also the main content of this paper. The two most widely studied and important applications are solid-state lasers and fluorescent lamps.

2. Electroluminescence: The process of converting electrical energy into light energy. This kind of luminescence does not have the process of first converting electrical energy into heat energy like an incandescent lamp, and then increasing the temperature of the object to emit light, so this kind of light is also called "cold light." The light emitted by a light emitting diode (LED) refers to the electroluminescence of a semiconductor. When current is applied to the p-n junction, it emits light. It has become an indispensable component in household appliances, but because it has not been able to emit high brightness, Long-life white light devices with relatively pure chromaticity have not been mass-produced.
3. X-ray and high-energy particle luminescence (radioluminescence): The luminescence process of an object excited by X-rays, γ -rays, protons, or neutrons. It is mainly used for ray detection and nuclear medicine imaging, etc.
4. Cathodoluminescence: The luminescence is produced by high-energy electron beam ionization and excitation of the luminescent center. The most common application is the TV display, of course, it also includes the display of computers, electron microscopes, and other electronic instruments. The electron beam is used to excite a luminescent substance so that the substance emits light, and the electricity used in the quantum energy is very high, usually in the thousands or even tens of thousands of electron volts (eV). After entering the luminous body, the high-energy electron beam hits the crystal lattice, producing an increasing number of secondary electrons. In the end, a large amount of electrons with only a few electron volts excites the luminescent material with the highest efficiency, and the material emits the strongest light.
5. Chemical luminescence: It mainly relies on the light radiation process triggered by the energy generated in the chemical reaction process. For example, when two separated compounds are placed in a transparent container when the separation is eliminated, the two substances are mixed to produce a chemical reaction, thereby producing light. This product can last for more than half an hour brightly and can be used for emergency lighting.
6. Bioluminescence: Chemical substances synthesized by cells, under the action of a special enzyme, convert chemical energy into light energy. Common ones are fish, fireflies, and bacteria, etc.

7. Triboluminescence: The luminescence phenomenon caused by mechanical action, such as crystals of tartaric acid and sucrose, flashes when they are squeezed.

1.1.2 Composition of luminescent materials

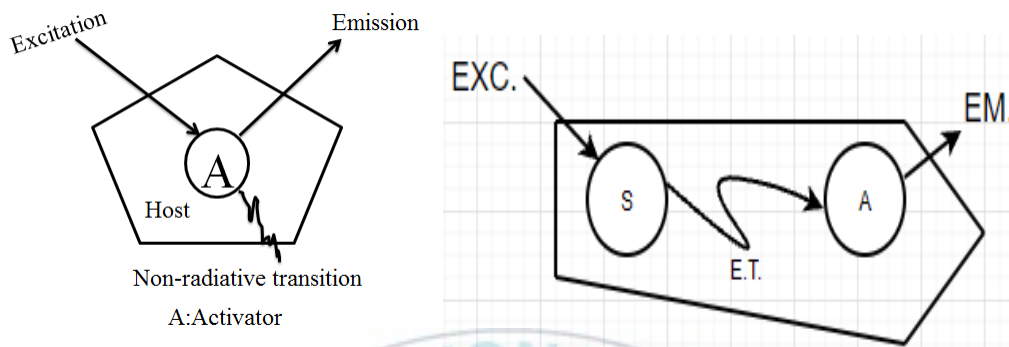


Figure 1.1 A luminescent ion A in its host lattice. Figure 1.2 Energy transfer from a sensitizer S to an activator A.

In general, solid luminescent materials consist of two parts: a luminescent center, an activator, and a host material. Figure.1.1 shows a schematic diagram of the luminescence behavior of photoluminescent materials (Example $\text{Al}_2\text{O}_3:\text{Eu}^{3+}$) [6-8].

Figure.1.1 demonstrates a simplified luminescence process consisting only of activator ions that absorb energy and produce luminescence and a host material for immobilizing the activator ions. In fact, in many cases, the part of the luminescent substance that absorbs energy is not only the activator ions, but also other ions and even the host material itself, and then other ions or host materials transfer the absorbed energy to the activator ions, and then the activator ions are excited to produce light. Absorbs energy other than activator ions and can transmit to activator. The ion of the agent is called a sensitizer. In actual research and development, we can try to absorb more efficient sensitizer ions other than multi-doping activator ions to improve the performance of light-emitting materials Figure.1.2.

Figure.1.3. and Figure.1.4. shows the schematic diagrams of the luminescence process and energy transfer are respectively given. The main physical processes which play a role in the luminescent material:

1. Absorption (excitation) which may take place in the activator itself, in another ion (the sensitizer), or in the host lattice.

2. Emission from the activator.
3. Nonradiative return to the ground state, a process which reduces the luminescence efficiency of the material.
4. energy transfer between luminescent centers.

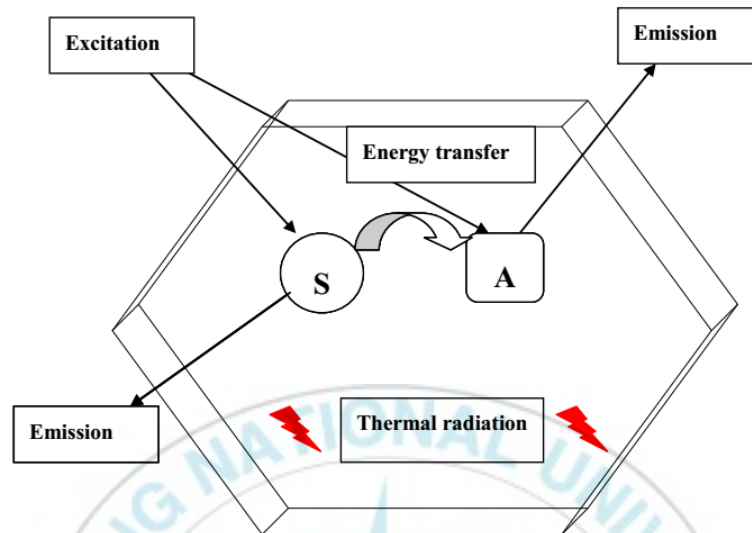


Figure 1.3 The main physical process of luminescence, M: matrix; S: sensitizer; A: activator.

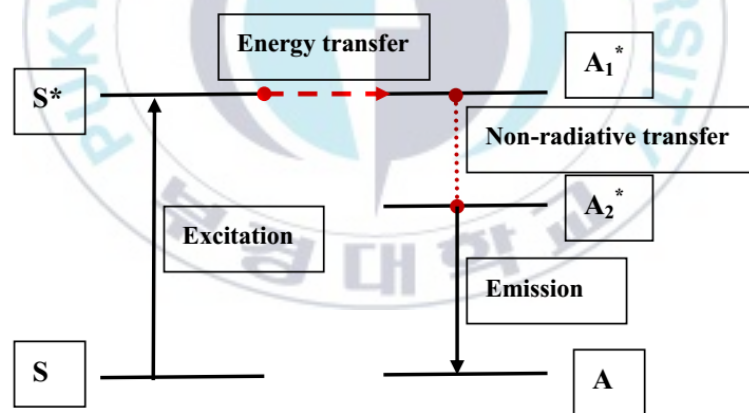


Figure 1.4. The energy transfer from sensitizer to activator, S: ground state of sensitizer; S*: excited state of sensitizer; A: ground state of activator; A1*, A2*: excited state of activator.

1.2 Rare earth luminescence

1.2.1 Rare earth ions

In 1794, the famous Finnish chemist Dolin discovered rare earth from silicon beryllium

yttrium ore, the properties of these rare earth elements are very similar. It has rich outer energy levels, a large radius, strong polarization, and active chemical properties. Its metal activity is second only to alkali metals and alkaline earth metal elements and is more active than other metal elements. However, rare earth elements are present in extremely complex mines, and it is difficult to separate them. Rare earth metal ions are the most widely used activator ions in luminescent materials. Phosphors currently on the market emit light from rare earth ions. Rare earth elements show stable physical and chemical properties due to their special electronic layer structure, as well as excellent magnetic, optical and electrical properties. It has a wide range of applications in military, aviation, electronics, medicine, new materials, glass ceramics and other fields [1, 9].

1.2.2 Electronic configuration of rare earth elements

The electron configurations of lanthanides are $1s^2 2s^2 2p^6 3s^2 3p^6 3d^{10} 4s^2 4p^6 4d^{10} 4f^n 5s^2 5p^6 5d^m 6s^2$ or $[Xe] 4f^n 5d^m 6s^2$ ([Xe] is the electron layer configuration of the noble gas xenon). It can be seen from the electronic configuration structure that the outermost 5d 6s electron configuration of each atom is the same, this is because when the rare earth element is in the atomic state, the electron fills the $5s^2 5p^6$ first, and then fills the 4f shell. In chemical reactions, rare earth elements easily lose three electrons in the 5d and 6s electron orbitals or 4f electron orbitals, showing +3 valence. The transitions between the 4f configuration levels of rare earth ions include (forced) electric dipole transitions and magnetic dipole transitions, which are characterized by linear transition radiation spectra and long fluorescence lifetimes. Since the 4f subshell is under the shielding of the outer $5s^2 5p^6$ full shell, it is little affected by the external environment, so the emission wavelength basically does not change with the change of the host material. The pair of 4f electronic transitions make rare earth ions have abundant energy level transitions, which can emit characteristic spectral lines in the range of ultraviolet, visible to near-infrared light regions, so rare earth ions can be used as active ions of luminescent materials [10-13].

Atomic number	Element name	Element symbol	Atom's electronic layer structure					Atomic radius/(nm)
			4f	5s	5p	5d	6s	
57	Lanthanum	La	0	2	6	1	2	0.1879
58	Cerium	Ce	1	2	6	1	2	0.1824
59	Praseodymium	Pr	3	2	6	0	2	0.1828
60	Neodymium	Nd	4	2	6	0	2	0.1821
61	Promethium	Pm	5	2	6	0	2	0.1810
62	Samarium	Sm	6	2	6	0	2	0.1802
63	Europium	Eu	7	2	6	1	2	0.2042
64	Gadolinium	Gd	7	2	6	0	2	0.1802
65	Terbium	Tb	9	2	6	0	2	0.1782
66	Dysprosium	Dy	10	2	6	0	2	0.1773
67	Holmium	Ho	11	2	6	0	2	0.1766
68	Erbium	Er	12	2	6	0	2	0.1757
69	Thulium	Tm	13	2	6	0	2	0.1746
70	Ytterbium	Yb	14	2	6	0	2	0.1940
71	Lutetium	La	15	2	6	1	2	0.1734

The inner layer is filled with 46 electrons

Table 1.1 The electron shell structure and radius of rare earth atoms

Table 1.1 lists the atomic radius and electron shell results of rare earth elements, in this table the characteristics of the electronic layer structure of these 15 lanthanide elements are: the outermost 6s orbital is filled with electrons, the 5s and 5p orbitals of the second outer layer are also in full electron state, and the 5d is an empty orbital or only one electron. The outer 4f is gradually filled from 0 until the last 4f orbital of lutetium is filled with 14 electrons. Since the distribution of the outermost and sub-outer electrons of various rare earth elements is similar, it is easy to lose two electrons in the outer 6s orbital and one d electron in the sub-outer layer (when there is no 5d electron, one 4f electron is lost), so Rare earth ions are usually positive trivalent. Dan Hongte's rule states that electrons arranged in the same electronic sublayer will always be distributed in different orbits as far as possible, and the spin direction is the same, so the number of 4f electrons has a very important influence on the valence state, $4f^0$, $4f^7$, $4f^{14}$ are Stable valence, while Ce^{3+} , Pr^{3+} , Tb^{3+} are easily oxidized to tetravalent, while Sm^{3+} , Eu^{3+} , and

Yb^{3+} are easily reduced to positive divalent [14, 15].

1.2.3 The unique spectroscopic characteristics of rare earth ions

Because photoluminescence mainly depends on the defect energy level in the crystal or the doping of impurity ions to form an effective luminescence center, rare earth elements have become the preparation of luminescence due to their unique electronic layer structure and spectral properties that are unmatched by general elements. The most ideal dopant ions can be selected from materials. Nowadays, rare earth luminescence covers almost the entire solid-state luminescence category.

The allowed optical transitions of the rare earth ions mentioned above are interconfigurational and consist of two different types, viz.

- ◇ Charge transfer transition ($4f^n \rightarrow 4f^{n+1}L^{-1}$, where L = ligand).
- ◇ $4f^n \rightarrow 4f^{n-1}5d$ transition.

Both are allowed, both have $\Delta R \neq 0$ and appear in the spectra as broad absorption bands. Charge transfer transitions are found for rare earth ions which like to be reduced, $4f-5d$ transitions for ions that like to be oxidized. The tetravalent rare earth ions (Ce^{4+} , Pr^{4+} , Tb^{4+}) show charge-transfer absorption bands. It has the following characteristics:

(1) The underfilled $4f/5d$ electron configuration will shield the outside world. The electron energy level is rich, the excited state life is long, and there are as many as 200,000 energy level transition channels, so it can produce a variety of radiation absorption and emission. The transition between different energy levels is subject to the law of spectral selection. Therefore, in the underfilled $4f$ electron sublayer, there are about 30,000 observable spectral lines that can emit various wavelengths from ultraviolet, visible light to infrared light. Electromagnetic radiation.

(2) Once the rare earth atoms lose their outer electrons and are in the state of ions, the $4f$ electron shell will be protected by the $5s^25p^6$ shell, so that the crystal field has little interference with the $4f$ electron shell. More importantly, the energy level difference of the $4f$ layer is extremely small, and the $f-f$ transition usually presents a sharp linear spectrum, which also causes the rare earth luminescent materials to have significant advantages such as narrow

emission bands, high color purity, and bright colors.

(3) The fluorescence lifetime can range from nanoseconds to milliseconds, spanning almost 6 orders of magnitude. Generally, the average lifetime of the excited state of atoms or ions is $10^{-10}\sim 10^{-8}$ seconds, and some rare earth elements can even reach $10^{-6}\sim 10^{-2}$ seconds due to the spontaneous transition between $4f$ electronic energy levels.

(4) High-temperature resistance, stable physical and chemical properties, and can withstand the action of high-power electron beams or high-energy rays.

(5) The ability to absorb excitation energy is strong, and the conversion efficiency is high. Based on the above excellent characteristics, rare earth luminescence can be widely used in many fields such as communications, luminous display, ultraviolet disinfection, medical care, and biomarking.

There are many types of rare earth luminescent materials, which can be roughly divided into two categories according to the role of rare earth in luminescent materials: The first category is rare earth ions as activators incorporated into crystal materials, and the second category can only be rare earth compounds or non-rare earth compounds. Rare earth ions used as activators can be said to be trivalent Eu^{3+} , Tb^{3+} , Dy^{3+} , and Sm^{3+} , etc., and can also be children's Eu^{2+} , and Nd^{3+} , Er^{3+} , Tm^{3+} , Ho^{3+} , Pr^{3+} , and Yb^{3+} are often used as activating ions or sensitizing ions for upconversion luminescent materials. Rare earth ions the type of luminescence has a decisive effect on the final luminescence characteristics, such as red phosphors or green upconversion luminescence used in white LEDs. The second category is that compounds containing rare earth ions such as La_2O_3 , Y_2O_3 , and Gd_2O_3 can be directly used as host materials, and include Compounds composed of rare earth and transition elements [15, 16].

1.2.4 4f-4f transitions

The rare earth ions are characterized by an incompletely filled $4f$ electron shell. The electrons are allowed to jump, and the optical radiation they emit comes from the energy release of the electron transition to the excited state and back to the ground state. This electronic transition inside the $4f$ electron layer is called f - f transition, and the luminescence of trivalent Eu^{3+} is also derived from this. Because the $5s$ and $5p$ electron layers are located outside the $4f$ electron layer,

they can shield the electrons located in the 4f layer, so when rare earth ions are doped in the matrix, the influence of the crystal field of the matrix on the electrons in the 4f layer is very weak, so the position of the emitted spectral lines is also very stable [17-20]. At the same time, the transition energy levels of rare earth ions in the crystal field of the matrix show similarities with free atoms, that is, discrete energy levels, so the shape of the emitted spectral lines is generally linear. The luminescence characteristics of the f-f transition of rare earth ions are summarized as follows:

1. The luminescence spectrum is linear, which is not affected by temperature.
2. Since the f electron is in the inner shell layer and is shielded by $5s^25p^6$, the matrix has little effect on the emission wavelength.
3. The light color is pure, the luminous color is stable, and it is not interfered by the external environment.
4. The temperature quenching is small, and it still emits light even at 400~500°C.
2. Abundant spectral lines, ranging from ultraviolet to infrared.
3. The concentration is small.
4. Long fluorescence lifetime.

1.2.5 4f-5d transitions

The f-d transition is a parity allowable transition, and its luminous intensity and transition probability are much greater than those of the f-f transition. The spectrum of this transition is closely related to the lattice vibration, so the spectrum emitted by the f-d transition is usually broadband. The main rare earth ions involved in the f-d transition are Ce^{3+} , Eu^{2+} , Yb^{2+} , Tb^{3+} , Sm^{2+} , Tm^{2+} , Dy^{2+} , Pr^{3+} and so on. For single-component broadband activator phosphors, Eu^{2+} and Ce^{3+} are the most suitable activators, and the broadband caused by their f-d transitions can cover part or all the visible spectrum of white LEDs. Since the 5d electrons are exposed to the outside, they are greatly affected by the surrounding crystal field environment [21, 22]. Accordingly, the position of the spectral band of the f-d transition will vary greatly depending on the environment. The characteristics of the f-d transition spectrum are as follows:

1. The emission spectrum is usually broadband.

2. Temperature has a greater influence on the emission spectrum.
3. Short fluorescence lifetime.
4. The emission spectrum is greatly affected by the host environment and can emit light of various wavelengths from ultraviolet to infrared.

1.2.5 Luminescence of Eu^{3+} ions

Trivalent europium ion (Eu^{3+}) as the most important rare earth ion of red phosphor activator is one of the most widely studied ions in the rare earth element family. The outer electronic structure of Eu^{3+} ions is $5p^64f^65d^0$, the 4f layer is sheltered by the $5s^25p^6$ electron layer, and is little affected by the external environment, while the emission lines of Eu^{3+} ions originate from the internal 4f-4f transition, so the luminescence performance is not affected by the external environment. The schematic diagram of the energy level transition of Eu^{3+} ion light emission is shown in Figure 1.5. When the Eu^{3+} ion is excited by the external energy, the electron transitions from the ground state to the excited state, and then from the excited state $^5\text{D}_0$ energy level back to the ground state $^7\text{F}_J$ ($J = 0, 1, 2, 3, 4$) energy levels, the energy will be emitted in the form of luminescence. The positions of the emission peaks corresponding to different transitions are different. The emission line of Eu^{3+} ion is a sharp linear spectrum, and its two main transitions are magnetic dipole transition $^5\text{D}_0 \rightarrow ^7\text{F}_1$ and electric dipole transition $^5\text{D}_0 \rightarrow ^7\text{F}_2$. Magnetic dipole transitions are not affected by local positional symmetry, whereas electric dipole transitions are very fragile at local symmetry positions and are called hypersensitive transitions. The location and environment of Eu^{3+} ions in the lattice have a direct impact on their emission properties. When the Eu^{3+} ion is located at the center of inversion symmetry in the lattice, $^5\text{D}_0 \rightarrow ^7\text{F}_1$ is the main transition mode, and the characteristic emission wavelength is in the range of 585-600 nm, emitting orange-red light; When inverting the position of the symmetry center, $^5\text{D}_0 \rightarrow ^7\text{F}_2$ is the main transition mode, and the characteristic emission wavelength is in the range of 610-630 nm, resulting in bright red light. The typical absorption band peaks of Eu^{3+} ions are around 395 and 465 nm, which are caused by the $^7\text{F}_0 \rightarrow ^5\text{L}_6$ and $^7\text{F}_0 \rightarrow ^5\text{D}_2$ transitions of Eu^{3+} , respectively [23-27].

Since the magnetic dipole transition $^5\text{D}_0 \rightarrow ^7\text{F}_1$ and the electric dipole transition $^5\text{D}_0 \rightarrow ^7\text{F}_2$ of

Eu^{3+} ions are very sensitive to the local environment, they can be used to probe the local structure of luminescent centers in a host lattice. The position occupied by Eu^{3+} in the luminescent material has high symmetry, and is dominated by magnetic dipole transition ${}^5\text{D}_0 \rightarrow {}^7\text{F}_1$; if the symmetry is low, it is dominated by electric dipole transition ${}^5\text{D}_0 \rightarrow {}^7\text{F}_2$, while other transitions are weak [27-30].

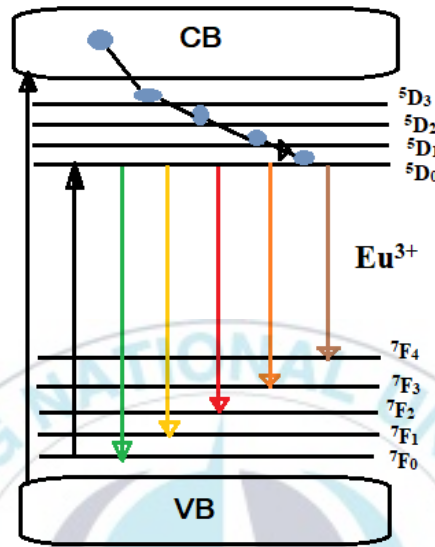


Figure 1.5. The schematic diagram of energy level transition in Eu^{3+} ion.

The host lattices of Eu^{3+} -doped luminescent materials $\text{NaLuO}_2:\text{Eu}^{3+}$ and $\text{NaGdO}_2:\text{Eu}^{3+}$ both have rock-salt structures, the difference is that Na^+ ions and Lu^{3+} (or Gd^{3+}) are arranged in different superstructures. In $\text{NaLuO}_2:\text{Eu}^{3+}$, the Eu^{3+} ion occupies the inversion symmetry site, and the ${}^5\text{D}_0 \rightarrow {}^7\text{F}_1$ magnetic dipole transition dominates (orange light) in its emission spectrum, as shown in Figure. 1.6(a). Eu^{3+} ions in $\text{NaGdO}_2:\text{Eu}^{3+}$ occupies the octahedral coordination center site, which is slightly deviated from the inversion symmetry center due to the superstructure [31]. Therefore, the ${}^5\text{D}_0 \rightarrow {}^7\text{F}_1$ electric dipole transition dominates (red light) in its emission spectrum, as shown in Figure. 1.6(b).

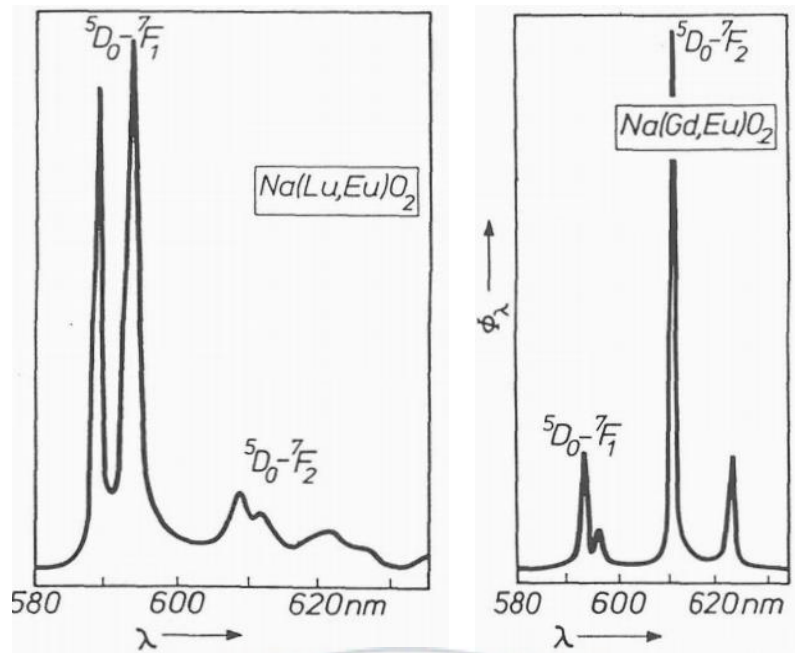


Figure 1.6 (a)(b) The emission spectrum of Eu^{3+} in NaLuO_2 and NaGdO_2 .

1.3 Transition metal Mn ion luminescence

For transition metals, the valence electron shell is $[\text{X}]3d4s$. The cations generally lose 4s electrons, the 3d electrons are exposed to the crystal field, and the incompletely filled d layer has an electron configuration of d^n . Due to the non-filled shell structure of transition metal ions, the energy gap from the ground state to the first excited state energy level is equivalent to the energy of optical photons, so transition metal ions are also widely used as activators for luminescent materials. Since the 3d electrons of transition elements are in the outer layer, they are very sensitive to the crystal environment and are greatly affected by external fields such as electric field, magnetic field, and coordination field. This is the biggest difference between rare earth ions [32, 33].

1.3.1 Luminescence of Mn^{2+}

The 3d shell of Mn^{2+} has 5 electrons, which is half-full and shows the largest atomic magnetic moment of all the elements. Compared with the f-orbital, the d-orbital has a stronger interaction with the environment and can exchange interactions with the carriers, thereby changing the spin of the carriers. The Mn^{2+} ion has an emission consisting of broadband whose position is strongly

dependent on the host lattice. The emission can vary from green to red. The decay time of this emission is on the order of milliseconds. Tetrahedral coordinated Mn^{2+} (weak crystal field) typically produces green emissions, and octahedral coordinated Mn^{2+} (stronger crystal field) emits orange to red emissions. The Tanabe-Sugano energy diagram of Mn^{2+} ion given in Figure 1.6. The ordinate in the figure is E/B , E is the crystal field energy, and the Δ/B represents the ratio of crystal field intensity Dq to electron Coulomb interaction B . By adjusting the crystal field strength, the spin-forbidden d-d transition (${}^4T_1 \rightarrow {}^6A_1$) of Mn^{2+} can be changed, and the emission can be changed from green to red [34-36].

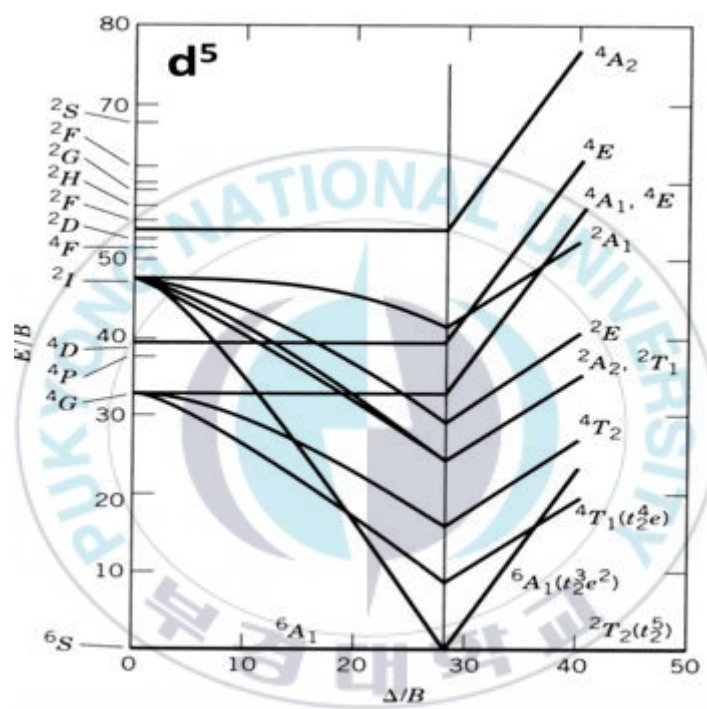


Figure 1.7 The Tanabe-Sugano energy diagram of Mn^{2+} .

1.4 Energy transfer

Energy transfer is essentially an ion transition. When excitation light acts on a luminescent material, it will cause the luminescent material to self-regulate. Changes in body energy, electrons and holes become unstable under the influence of excitation light, or some ions are excited to higher energies state. Therefore, the excited state will transfer, interact with adjacent ions to transfer energy, and electrons and holes are not limited in the original position, the energy is transferred from the excited state to the ground state or from the ground state to the

excited state, forming a readjustment of the energy redistribute [37-40].

(1) Self-absorption

After a part of the crystal emits light, the emission spectrum coincides with the absorption spectrum, causing the light wave to be absorbed by the crystal itself, this phenomenon is called self-absorption. Photons in light waves transport energy at a higher speed, and the process distance is not fixed, but the transmission not affected by temperature.

(2) Resonance transfer

The most common luminescence of solid-state materials is resonance transfer, which means that under the action of near-field force or electron exchange, the excited state, the process by which a center transfers resonance energy to other centers. The two energy transfer values are not much different, and this process is related to the temperature correlation is small.

(3) Carrier energy transfer

The diffusion drift of carriers is the energy transfer medium in insulators and semiconductor photoconductive materials, and the transfer process will generate electricity flow and electrical photoconductive phenomena are closely related to temperature.

(4) Exciton energy transfer

The excitons in the lattice can move freely, and the energy transfer of excitons is mainly divided into two types. The first is excitons reabsorption with other centers transfers the activation energy, and the other is the intrinsic excitation energy of excitons from A to B. The critical distance R_c can be used to judge the energy transfer mode of the luminescent material. During the process of energy transfer, the excitation on the one hand, the hair-state center transitions back to the ground state through its own radiation, and the probability at this time is P_1 ; on the other hand, it can transfer the energy to the ground state is P_2 . when $P_1=P_2$, the distance at 2 is called the critical distance R_c .

1.5 Implementation of white light diodes

White light LEDs were previously realized by white light (polymorph) mixed with red, green, and blue primary color chips. Now gradually converted to white light (single crystal form) obtained by exciting the corresponding phosphor with a chip [41-43].

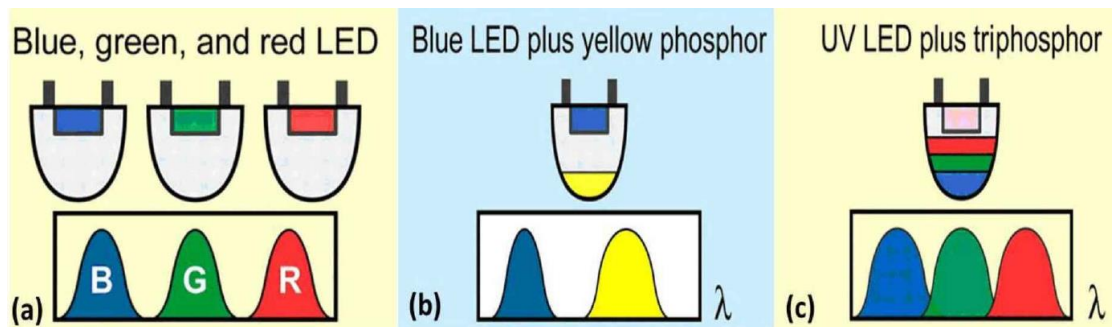


Figure 1.8 Three methods of generating white light. (a) red + green + blue-LEDs; (b) UV-LED + RGB phosphors; (c) blue-LED + yellow phosphor.

1) UV-near UV LED excitation of mixed red, green and blue phosphors

Red, green and blue phosphors are filled outside the excitation chip, and the ultraviolet-near-ultraviolet LED chip is used to stimulate at the same time, and white light can also be formed after the three colors of light are mixed.

2) Blue LED mixed with red and green phosphors

White light can also be formed by simultaneously exciting red and green phosphor luminescent materials with a blue LED chip. The white light produced by this method has three basic colors: red, green and blue, and has the advantages of high color rendering, high light conversion efficiency, long working time and simple preparation procedure, but the overall luminous efficiency is low, the color temperature is high, and at least two kinds of phosphors are required, which increases the production cost.

3) Multi-chip combination to achieve white light

The multi-chip combination method combines three different light-emitting diode chips of red, green and blue, and uses a lens to mix the chips to emit light of different colors to form white light. The advantage of this method is that the white light emitted can be controlled manually, with very high color rendering, but the disadvantages are also obvious, that is, it consumes a lot of materials, driving voltage and operating temperature there may be differences due to the influence of the environment and its performance, and because the current required by each chip is different, three sets of circuits need to be designed, which will inevitably increase the design difficulty and cause a corresponding increase in cost. Because of this, this method is not suitable for large-scale use and is limited in application. Today's commercial implementation is mainly a single-chip type.

1.6 Scopes of this thesis

Over the past few years, phosphors, as a key and technologically important component of LEDs, have been recognized as a prerequisite for the functionality and success of many lighting and display systems.

(1) Due to the structural characteristics of the electrons in the 4f layer, rare earth ions show extremely rich energy level transition forms, which can absorb or emit light from the ultraviolet to the infrared region, thereby forming a variety of luminescent materials. Therefore, rare earth luminescent materials play an increasingly important role in social development and scientific and technological progress.

(2) Eu^{3+} is one of the most widely studied ions in the rare earth element family, and it is also the most important rare earth ion as an activator for red phosphors. The typical absorption band peaks of Eu^{3+} ions are around 396 and 465 nm, which can be well matched with commercial n-UV and blue LED chips. In addition, since the magnetic dipole transition ${}^5\text{D}_0 \rightarrow {}^7\text{F}_1$ and the electric dipole transition ${}^5\text{D}_0 \rightarrow {}^7\text{F}_2$ of Eu^{3+} ions are very sensitive to the local environment, it can also be used as an ideal fluorescent probe to analyze the symmetry of lattice positions.

(3) Mn^{2+} emission peak is generally broad band, with an emission peak around 550 nm to 750 nm, which originates from the ${}^5\text{T}_1 \rightarrow {}^6\text{A}_1$ transition spin forbidden d-d transition. According to the Tanabe-Sugano figures, the emission peaks of Mn^{2+} in the octahedral coordination environment are located on the orange to red region. The emission peak is located on the green region when Mn^{2+} is in the tetrahedral coordination environment. By adjusting the crystal field strength, the spectrum of transition metal Mn^{2+} changes from green to red.

2. Experimental and Characterization

2.1 Sample preparation

2.1.1 Synthesis of $\text{Ca}_3\text{WO}_5\text{Cl}_2$ and Eu^{3+} doped $\text{Ca}_3\text{WO}_5\text{Cl}_2$

$\text{Ca}_3\text{WO}_5\text{Cl}_2$ phosphors were synthesized via the facile solid-state reactions. The raw reactants

are CaCO_3 (99.9%), WO_3 (99.9%) and NH_4Cl (99.9%). Firstly, CaCO_3 and WO_3 with the stoichiometric weight were ground by ball-milling in alcohol medium for 4 h. The slurries were dried in a drying oven and then were calcined at $850\text{ }^\circ\text{C}$ for 6 h to obtain the precursor Ca_2WO_5 . Secondly, the powders were thoroughly ground again with adding the CaCl_2 (99.9%) powders and then sintered at $800\text{ }^\circ\text{C}$ for 6 h to obtain the final products $\text{Ca}_3\text{WO}_5\text{Cl}_2$.



2.1.2 Synthesis of $\text{Na}_2\text{Mg}_{1-x}(\text{PO}_3)_4:x\text{Mn}^{2+}$ ($x=0.01, 0.03, 0.05, 0.07, 0.09, 0.11$)

The phosphors of $\text{Na}_2\text{Mg}_{1-x}(\text{PO}_3)_4:x\text{Mn}^{2+}$ ($x=0.01, 0.03, 0.05, 0.07, 0.09, 0.11$) phosphor were prepared by high-temperature solid-state reaction. The raw reactants are Na_2CO_3 (99.9%), $4\text{MgCO}_3\cdot\text{Mg}(\text{OH})_2\cdot 5\text{H}_2\text{O}$, $\text{NH}_4\text{H}_2\text{PO}_4$ (99.9%), MnCO_3 (99.9%). All the starting reagents were mixed in stoichiometric ratios and ground in an agate mortar for 20 minutes to obtain the homogeneous mixture. Then, the mixture was calcined at $400\text{ }^\circ\text{C}$ for 10 h in a crucible in atmosphere. The obtained mixture was reground carefully and maintained at $850\text{ }^\circ\text{C}$ for 8.5 h in a muffle furnace. Thus, a series of the Mn^{2+} -doped $\text{Na}_2\text{Mg}(\text{PO}_3)_4$ phosphors were successfully obtained as cooling down to room temperature.

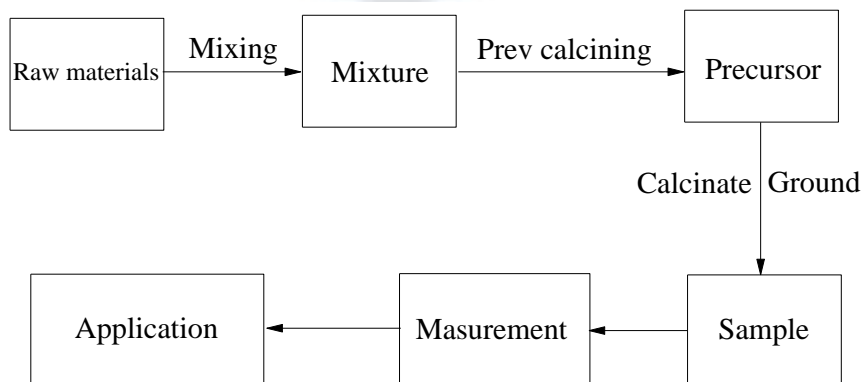


Figure 2.1 The preparation process of the high-temperature solid-state method.

2.2 Material Characterization

2.2.1 X-ray Diffraction

X-ray powder diffraction is an optical analysis method detected by an instrument. Monochromatic X-rays are irradiated on a powder crystal sample. If the angle between the orientation of a group of facets of one of the crystal grains and the incident X-ray is θ , the diffraction condition is satisfied. condition, diffraction occurs at the diffraction angle 2θ . There are multiple grains in the sample and the diffraction is satisfied. By using the detector of the powder crystal diffractometer to rotate around the sample at a certain angle, all diffraction lines of different mesh planes and different orientations in the powder crystal are received, and the corresponding diffraction pattern is obtained. By performing X-ray diffraction on the material and analyzing its diffraction pattern, it is a research method to obtain the composition of the material, the structure or morphology of the atoms or molecules inside the material, etc., but there is low sensitivity, and the required sample content is greater than 1%. Generally, tens to hundreds of millimeters are required, and problems such as amorphous samples cannot be analyzed.

Bragg equation:

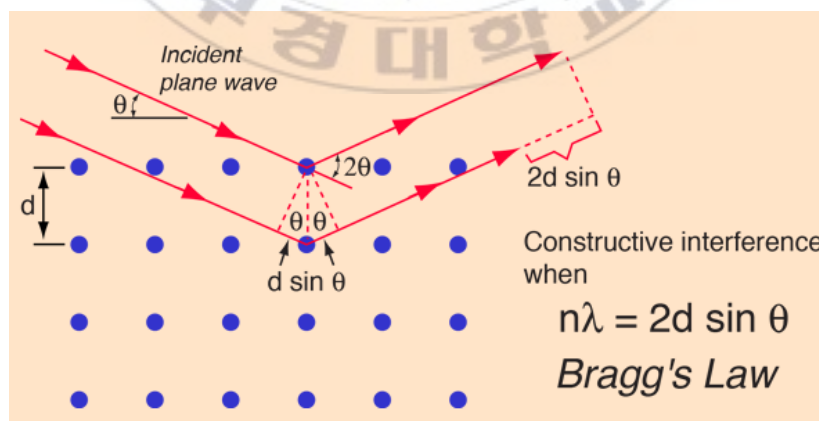


Figure 2.2 Schematic diagram of Bragg's Law.

$n\lambda = 2d \sin \theta$ (λ is the X-ray wavelength, n is the diffraction order, d is the interplanar spacing, and θ is the diffraction half angle.) When a monochromatic X-ray irradiates a powder crystal sample, if the angle between the orientation of the network plane (hkl) and the incident X-ray

is θ , and if the diffraction conditions are met, diffraction occurs at the diffraction angle 2θ (the angle between the diffraction line and the extension of the incident X-ray).

The phase structures of the samples prepared in this paper were taken on a Rigaku D/Max diffractometer (40 kV, 30 mA) with Bragg-Brentano geometry using Cu-K α 1 radiation ($\lambda = 1.5405 \text{ \AA}$). The XRD data in 2θ ranging from 10° to 70° were collected at a scanning mode with a step size of 0.02° and a rate of $4.0^\circ \text{ min}^{-1}$.

2.2.2 Scanning Electron Microscopy

Scanning Electron Microscope (SEM) is a structural analysis tool, the principle of which is to use an electron beam as a light source to focus the electron beam is irradiated on the sample through a raster-like scanning method, so as to reflect various information of the produced sample, and then by collecting information and processing, the micro-topography is obtained. SEM provides high resolution, long depth of field and rich imaging. Therefore, the image research method of scanning electron microscope is used to analyze the microstructure, which is rich in content and intuitive in method. Surface observation and analysis of various materials.

In this study, the surface morphology of powder samples is mainly analyzed. When preparing powder samples, first of all Adhere conductive glue on the tray, then place a small amount of dried powder sample on the conductive glue and use a blowing rubber ball to the tray was blown radially outwards to distribute the powder evenly on the tape, gold sprayed before testing, and finally the morphologies of the samples at different resolutions were measured with a Philips XL230 scanning electron microscope.

2.2.3 Photoluminescence Emission and Excitation Spectroscopy

When a luminescent material is excited by excitation light of a specific wavelength, the relationship between the emission intensity or energy of the emitted light and the wavelength of the emitted light is the emission spectrum. If it is a graph of emission intensity versus wavelength, the spectral lines can be broad-band, narrow-band or linear depending on the nature of the luminescent material. And if the relationship between the energy of the emitted

light and the wavelength of the luminescent material is excited by the excitation light of a specific wavelength, the emission intensity or the relationship between the energy and the wavelength of the emitted light shows the energy distribution of the emitted light. Excitation spectrum refers to the relationship between the intensity of the emission line at this wavelength and the excitation wavelength by monitoring a specific emission wavelength under the excitation of light of different wavelengths. It reflects the luminescence effect of materials excited by light of different wavelengths and can know the characteristic absorption peak range of matrix and activator ions. Therefore, the optimal excitation wavelength range of materials can be determined by excitation spectrum, which is of great significance for the application of research materials.

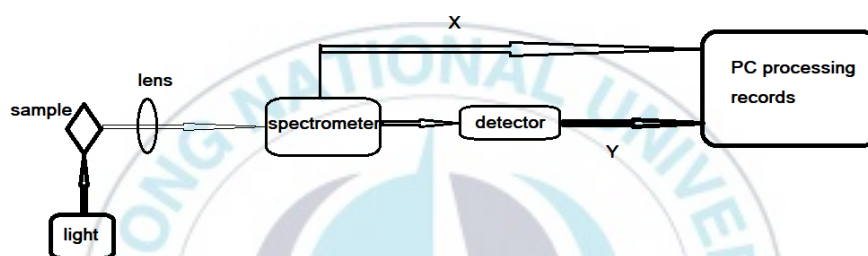


Figure 2.3 Measurement schematic of excitation spectrum.

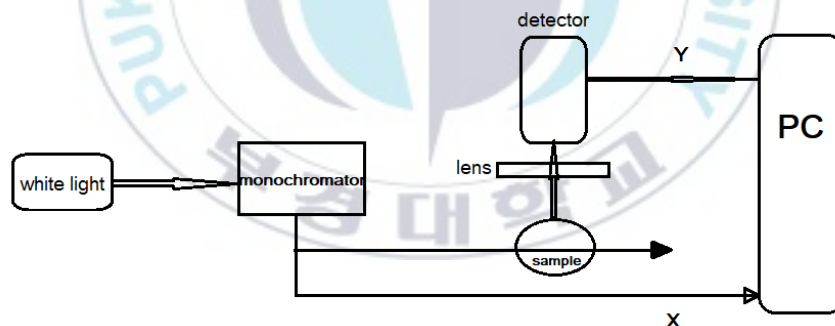


Figure 2.4 Measurement schematic of emission spectrum.

The photoluminescence (PL) excitation and emission spectra of the phosphors were measured on a luminescence spectrometer (Perkin-Elmer LS-50B). The luminescence was investigated in the temperature region from 10 to 480 K. The samples were fixed in the vacuum specimen chamber with liquid helium flow. The excitation source is 266 nm created from the fourth harmonics of pulsed Nd-YAG laser. A digital storage oscilloscope (500 MHz, Tektronics TDS754A) was used to record the dynamic data in this study.

2.2.4 Fluorescence Decay Time

The fluorescence lifetime of the sample means the time interval between the phosphors excitation and the detection of emitted light. The fluorescence lifetime is strongly related to the lifetime of excited states. Under fixed excitation and emission wavelength pulsed laser irradiation, the sample generates a certain fluorescence signal. decay time (τ) there are generally two common forms of decay, exponential decay, and non-exponential decay.

1) exponential decay, luminescence intensity $I(t)$:

$$I = I_0 \exp(-t/\tau) \quad (2.1)$$

where I_0 is the luminous intensity, t is the time, and τ is the decay lifetime. After τ seconds, the luminescence intensity decreased to $1/e$ of the intensity before excitation was stopped. After the external excitation stops, the electrons in the excited state transition back to the ground state to produce luminescence, and the decay curve presents a single exponential decay. Taking the decay time as the abscissa and the logarithm of the luminescence intensity as the ordinate, a straight line is obtained by fitting with Origin software. The slope is $1/\tau$, which gives the decay lifetime.

2) non-exponential decay, the lifetime obtained by fitting the formula:

$$\tau_{average} = \frac{\int_0^{\infty} I(t)tdt}{\int_0^{\infty} I(t)dt} \quad (2.2)$$

where t is the time, $I(t)$ is the luminous intensity at time t after the excitation cut-off, and $\tau_{average}$ is the average decay lifetime. Generally, when a material emits light, there will be non-exponential decay due to thermal activation energy migration.

In this study the fluorescence decay curve test used a pulsed YAG:Nd laser as an excitation source.

2.2.5 Temperature dependent photoluminescence

The thermal stability of with the optimum composition was evaluated by recording the emission spectra at different temperatures. The low temperature dependence of the luminescence spectra was determined by cooling each sample in a closed loop He cryostat to

~10 K and then gradually heating to room temperature. When testing high temperature-dependent luminescence, the phosphor was placed on an aluminum plate with a cartridge heater and heated with a thermal sensor until the temperature stabilized and the test was measured from room temperature to 480 K.

2.2.6 Color Coordinate

Chromaticity coordinates, abbreviated as CIE, is an important physical method to describe color objectively and quantitatively, which effectively avoids errors caused by human observation. Any color can be represented by chromaticity coordinates it can be quantitatively represented by the three primary colors blue (x), green (y), and red (z). (2.3), (2.4) and (2.5) to represent:

$$x = X/(X + Y + Z) \quad (2.3)$$

$$y = Y/(X + Y + Z) \quad (2.4)$$

$$z = Z/(X + Y + Z) \quad (2.5)$$

where x , y , and z are the chromaticity coordinates, and X , Y , and Z are the three primary color stimulus values. Since $x+y+z=1$, (x , y) can be used to represent the coordinates of a color.

As shown in the CIE chromaticity diagram, according to the National Television System Committee (NTSC), the standard blue CIE coordinates are (0.14, 0.08), the standard green CIE coordinates are (0.21, 0.71), and the standard red CIE coordinates are (0.67, 0.33). The CIE coordinates involved in this work are to calculate and process the obtained luminescence spectrum data through the Color Coordinate software to obtain the coordinate value of the phosphor, and then input the coordinate value into the CIE1931 software, so that the color of the phosphor can be clearly seen.

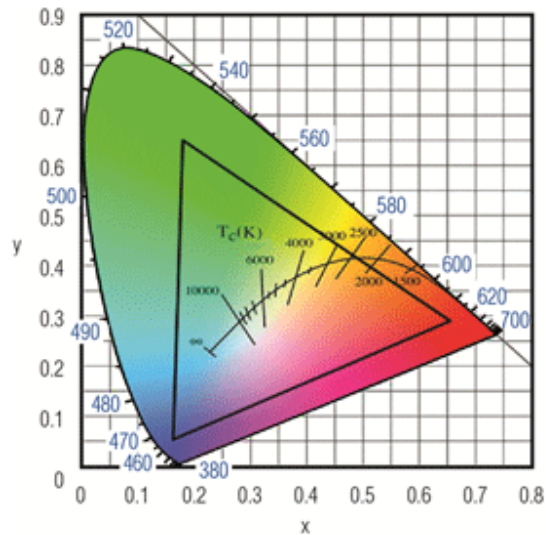


Figure 2.5 This CIE gamut chart shows the x,y chromaticity coordinates and color temperature locus. The triangular area covers the gamut of colors defined by standard green, red, and blue colors.

2.2.7 Thermal stability activation energy

when the phosphor is in a high-temperature state for a long time, the fluorescence intensity will gradually decrease with the increase of temperature, that is, the temperature quenching effect occurs. At the same time, in the use of phosphors, the temperature of the phosphors will change due to long-term excitation and changes in the working environment. With the change the temperature, the luminous efficiency and color coordinates of the phosphors may be changed. Thermal stability testing of phosphors is an important step to measure the performance of phosphors. Activation energy E_a refers to the energy required for a molecule to change from a normal reactant to an activated molecular state, which can determine the thermal stability of the phosphor. The higher the activation energy, the stronger the thermal stability. The activation energy can be calculated from the following equation as:

$$\ln \frac{I_0}{I} - 1 = \ln A - \frac{\Delta E}{kT} \quad (2.6)$$

Where I_0 represents emission intensity of the phosphors at first, I is emission intensity at temperature T , A is a constant, ΔE is the activation energy and k is the Boltzmann constant (8.63×10^{-5} eV).

3. Synthesis, crystal structure and luminescent properties of Eu^{3+} -activated halotungstates applied in W-LEDs

3.1 Introduction

Tungstate families as the candidates of RE-free full-color phosphors have drawn increasing attention due to their admirable merits of large X-ray absorption coefficient, high chemical stability, high energy transfer efficiency and high light yield [44]. The highly charged central transition-metal ions W^{6+} surrounded by several ligand ions are known as an important class of self-activated luminescent matters, which feature the luminescence arising from the charge-transfer transition from anion ligand to the d^0 electronic-configuration central metal ion. For example, CaWO_4 [28], $\text{CsGa}_{0.333}\text{W}_{1.667}\text{O}_6$ [45], $\text{A}_2\text{W}_3\text{O}_{10}$ ($\text{A} = \text{Rb}$ and Cs) [46, 47] etc. Although the self-activated tungstate has been widely investigated, many reports have been concerned on non-contact optical thermometry for temperature remote detection, which is based on the fact that temperature has great and subtle influences on the luminescence characteristics such as the peak wavelength and bandwidth, emission intensity, luminescence intensity ratio, fluorescence lifetime, up-conversion, and decay rise time etc. [27, 48-51].

Some rare earth Eu^{3+} ion-doped tungstate that can be excited by near-ultraviolet and blue light produce highly efficient red phosphors that can be used as red phosphors for white LEDs. On the one hand, tungstate is chemically stable and has a broad and strong charge transfer absorption band in the near-ultraviolet region. After ultraviolet excitation, its energy can be transferred to the activator ions through non-radiative transitions, and it is a good host for rare earth activator Eu^{3+} . On the other hand, Eu^{3+} has unique spectral properties due to its special 4f electronic configuration, which can emit red fluorescence with good monochromaticity and high quantum efficiency and is widely used in lighting and display. When Eu^{3+} ions are located on the asymmetric lattice sites of tungstate, a ${}^5\text{D}_0 \rightarrow {}^7\text{F}_2$ transition can be performed, resulting in red emission at a wavelength of about 616 nm. Therefore, Eu^{3+} -doped tungstate and molybdate are expected to be used as red light-emitting materials for light LEDs [52].

This work reports a novel luminescence property of the self-activated halotungstates

$\text{Ca}_3\text{WO}_5\text{Cl}_2$ phosphors. The temperature-dependent luminescent properties were characterized in detail for the first time. The experimental results show that $\text{Ca}_3\text{WO}_5\text{Cl}_2$ phosphors are potential candidates for UV-based self-activated luminescent materials and can be applied in the field of white light diodes with high thermal stability.

3.2 Results

3.2.1 Structural and properties of pure $\text{Ca}_3\text{WO}_5\text{Cl}_2$

The Rietveld refinement analysis of the XRD patterns of as-synthesized $\text{Ca}_3\text{WO}_5\text{Cl}_2$ were shown in Figure.1.1. The detailed crystallographic data and structural parameters, extracted from the Rietveld refined XRD data, were summarized in Table 3.1, and the position, thermal parameter (Biso), and occupancy of the constituent atoms are summarized in Table 3.2. The experimental data (black square) is expected to be matched well with the calculated data (red line), as represented by the goodness of fittings. $\text{Ca}_3\text{WO}_5\text{Cl}_2$ crystallize in orthorhombic crystal structure, and the unit cell parameters are $a=11.820(2)$ Å, $b=11.132(1)$ Å, $c=5.587(1)$ Å, $V=735.14(19)$ Å³, and $Z=4$ for $\text{Ca}_3\text{WO}_5\text{Cl}_2$ with the space group of Pnam (62). The refined XRD pattern of as-precipitated $\text{Ca}_3\text{WO}_5\text{Cl}_2$ is consistent with the standard data (ICSD#2335), indicating a high purity and crystallinity [53].

Accordingly, the crystal structure of $\text{Ca}_3\text{WO}_5\text{Cl}_2$ is isostructural with the mineral pinalite $\text{Pb}_3\text{WO}_5\text{Cl}_2$ [54], as shown in Figure 3.2. Figure 3.2c illustrates the crystal structure of the WO_5Cl unit cell, where the W^{6+} ion is surrounded by five oxide ions and one chloride ion, forming a heavily distorted WO_5Cl octahedron. And the WO_5Cl octahedra do not share their anions, keeping the nearest-neighbor distance of 6.3793 Å, which is longer than 5 Å and results in localized 5d electrons with small electron transfers [54].

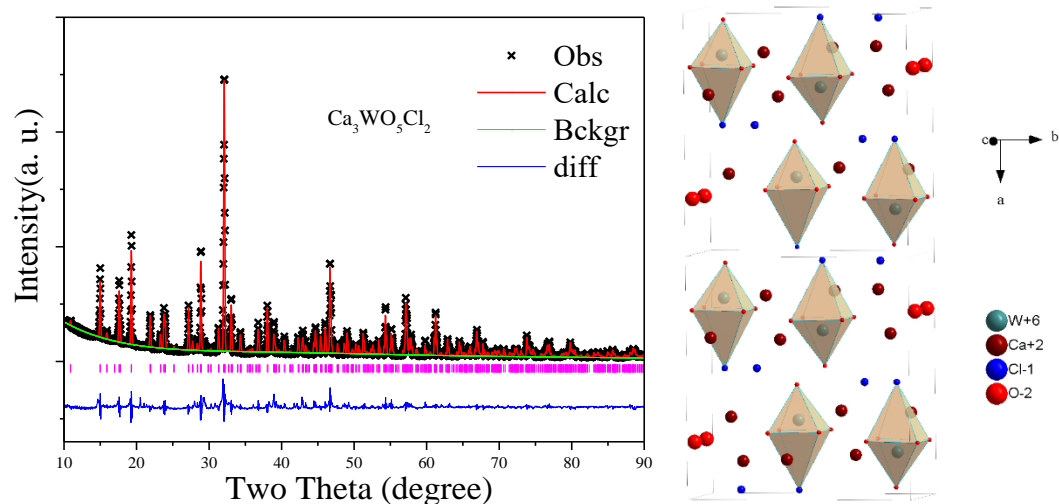


Figure 3.1 Experimental (black point) and calculated XRD patterns (red solid line) and their differences (blue solid line) for the Rietveld fit of the $\text{Ca}_3\text{WO}_5\text{Cl}_2$ phosphor. The short vertical lines (pink line) show the position of Bragg reflections of the calculated patterns. Figure 3.2 The configuration of the atoms in crystal structures $\text{Ca}_3\text{WO}_5\text{Cl}_2$.

Table 3.1 the refined crystal parameters of $\text{Ca}_3\text{WO}_5\text{Cl}_2$ and compared with the standard data.

Formula	Standard- $\text{Ca}_3\text{WO}_5\text{Cl}_2$	Refined- $\text{Ca}_3\text{WO}_5\text{Cl}_2$
symmetry	Orthorhombic	Orthorhombic
space group#	$C m c m$ (63)	$P n a m$ (62)
$a/\text{\AA}$	5.796(2)	11.820(2)
$b/\text{\AA}$	13.825(2)	11.132(1)
$c/\text{\AA}$	11.469(2)	5.587(1)
Z	4	4
$V/\text{\AA}^3$	919.01(38)	735.14(19)
W-O1(\AA)	1.7516	1.7243
W-O2(\AA)	1.9042	1.9112
W-O3(\AA)	1.9042	1.8875
W-O4(\AA)	1.9042	1.9112
W-O5(\AA)	1.9042	1.8875
W-Cl1(\AA)	3.4424	3.4039
Δ	-	1.2097
W1-W1(\AA)	6.4263	6.3793
R_p	-	0.0174
R_{wp}	-	0.0152
χ^2	-	1.279

3.2.2 Self-activated luminescence of the $\text{Ca}_3\text{WO}_5\text{Cl}_2$

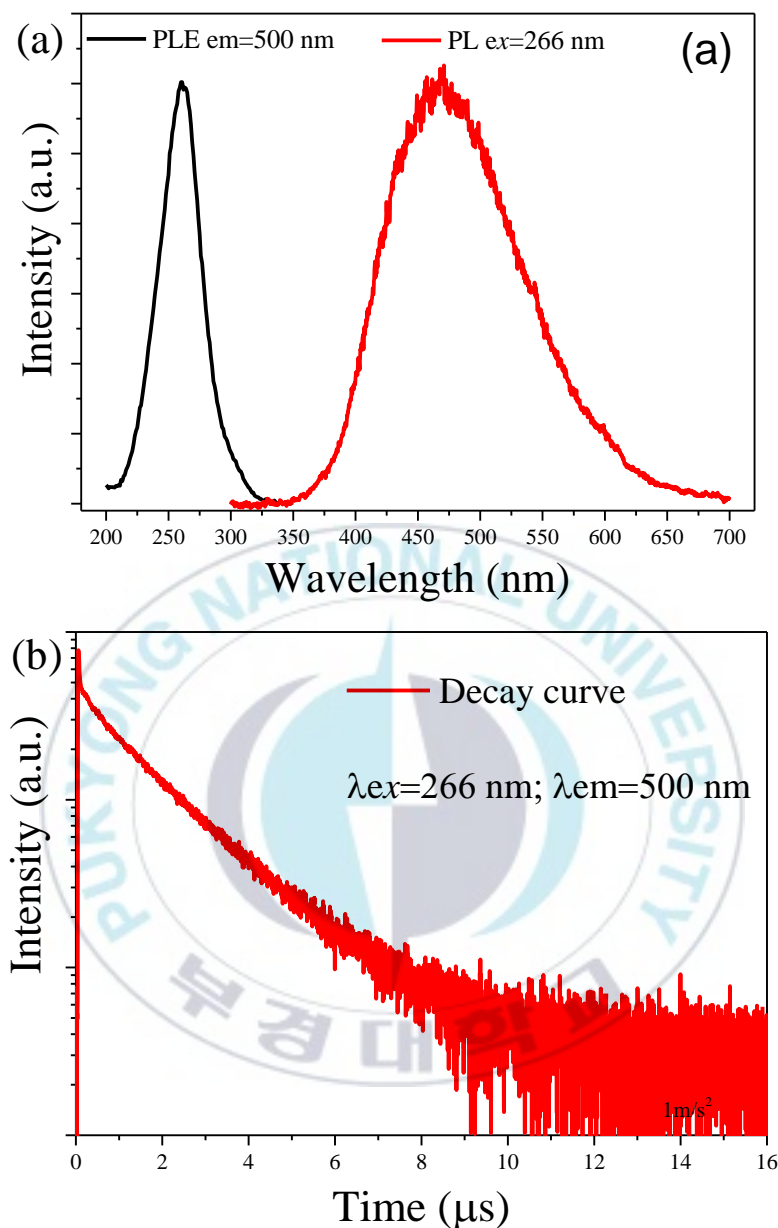


Figure 3.3 (a) The room temperature PLE and PL spectra of host ($\text{Ca}_3\text{WO}_5\text{Cl}_2$ phosphor) ($\lambda_{\text{em}} = 560 \text{ nm}$ and $\lambda_{\text{ex}} = 266 \text{ nm}$), and (b) the decay curves of host ($\text{Ca}_3\text{WO}_5\text{Cl}_2$ phosphor) ($\lambda_{\text{em}} = 704 \text{ nm}$; $\lambda_{\text{ex}} = 344 \text{ nm}$).

Tungstate crystals belong to the self-activated luminescent family, the PL and PLE spectra of $\text{Ca}_3\text{WO}_5\text{Cl}_2$ were characterized as shown in Figure. 3.3(a). The emission spectrum, excited by 266 nm, consists of an intense ultra-broad band covering the entire visible region in which the peak maximum centered at 475 nm. Whereas the corresponding PLE spectrum, monitored by 500 nm, exhibits a broad absorption band in the ultraviolet (UV) region ranging from 200 to 330 nm, with a maximum at 270 nm. Usually, the luminescence of tungstate compounds

originates from the tetrahedral WO_4^{2-} group or the octahedral WO_6^{6-} group due to the charge transfer transition from 2p orbital of the O^{2-} ligand to the 5d orbital of the d^0 tungsten metal ion. The $[\text{WO}_5\text{Cl}]^{5-}$ group and the WO_6^{6-} group have analogous octahedral symmetry, and the band shape of the excitation and emission spectra of pure $\text{Ca}_3\text{WO}_5\text{Cl}_2$ is similar to the reported AgGdW_2O_8 with octahedral WO_6^{6-} group. This indicates that the charge transfer process in WO_6^{6-} group occurs also in $[\text{WO}_5\text{Cl}]^{5-}$ group.

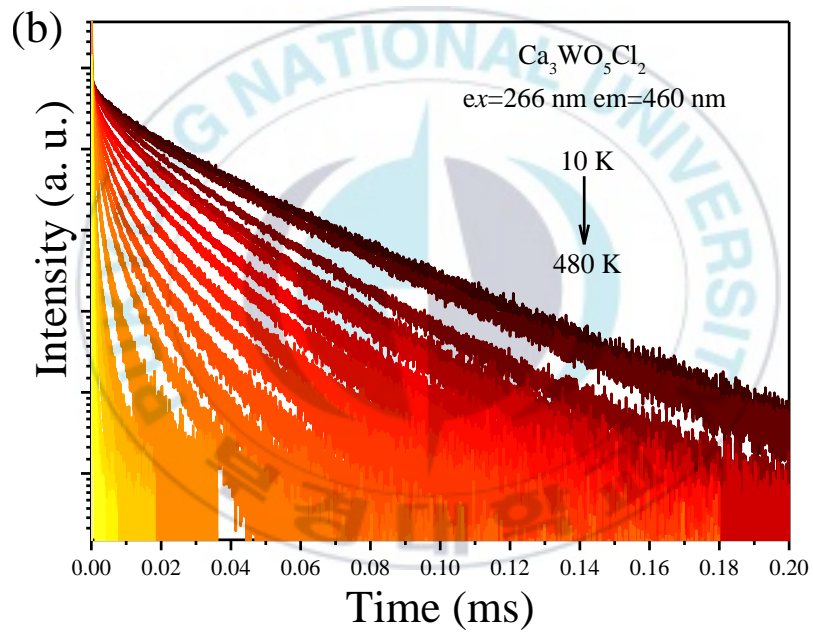
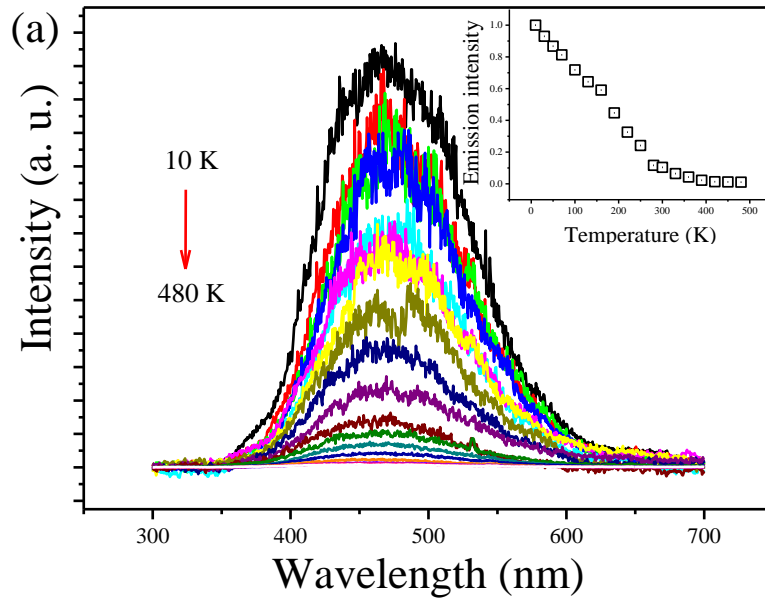
The decay curves of the $\text{Ca}_3\text{WO}_5\text{Cl}_2$ excited by 266 nm and monitored by 500 nm at temperature are shown in Figure. 3.3(b). The decay curve is slightly nonexponential which seems existence of two decay components, we fit the decay with a double exponential function. The anomalous decay phenomenon is also reported in self-activated NaWO_2PO_4 [55] phosphor by Blasse et al. The average decay time can be calculated by the following equation:

$$\tau_{\text{avg}} = \frac{\int tI(t)dt}{\int I(t)dt} \quad (3.1)$$

The average luminescence decay time was calculated to be 8 μs , which is comparable to other reported self-activated tungstates in Table 3.2.

Table 3.2 Decay times of $\text{Ca}_3\text{WO}_5\text{Cl}_2$ and some fitting parameters of some luminescent tungstate compounds.

Compound	τ_{21}/τ_{31} (μs)	ϵ cm^{-1}	E cm^{-1}	Ref.
NaWO_2PO_4	550/80	24	/	[55]
CaWO_4	330/8	20	/	[56]
$\text{Na}_2\text{W}_2\text{O}_7$	200/30	12	/	[57]
$\text{Ba}_2\text{WO}_3\text{F}_4$	222/33	10	/	[58]
$\text{PbWO}_4:\text{Mo}$	243/12	2.82	2095	[59]
$\text{Cs}_2\text{WO}_2\text{F}_4$	456/99	29	2261	[60]
$\text{Ca}_3\text{WO}_5\text{Cl}_2$	12/48	102	1828	This work



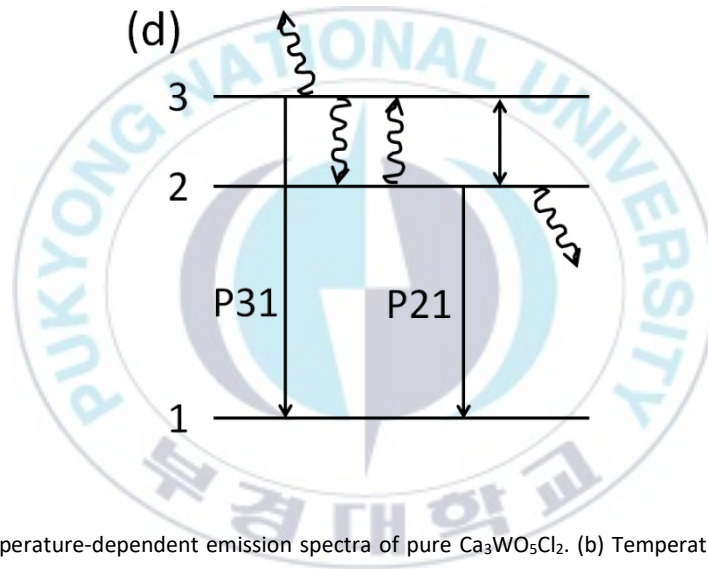
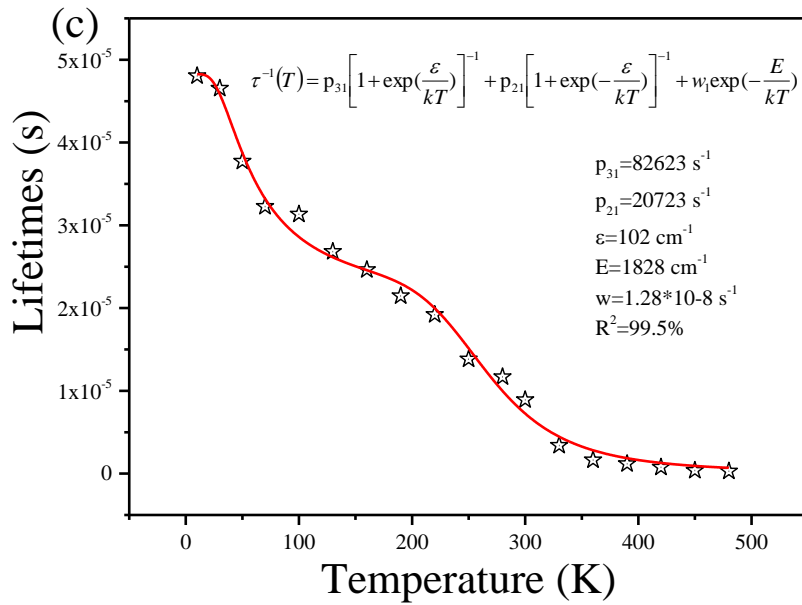


Figure 3.4. (a) Temperature-dependent emission spectra of pure $\text{Ca}_3\text{WO}_5\text{Cl}_2$. (b) Temperature-dependent decay curves of pure $\text{Ca}_3\text{WO}_5\text{Cl}_2$. (c) Calculated lifetime of pure $\text{Ca}_3\text{WO}_5\text{Cl}_2$. (d) Three-level energy scheme.

Figure. 3.4(a) displays the temperature dependent emission spectra of $\text{Ca}_3\text{WO}_5\text{Cl}_2$. From the temperature dependent calculated emission intensities insert in Figure. 3.4(a), it is seen that emission intensity is reduced with increase in temperature. Such reduction due to thermal quenching wherein emissive centers are thermally activated through the crossing point between the ground and the excited levels are well known [61].

The decay curves of the $\text{Ca}_3\text{WO}_5\text{Cl}_2$ as a function of temperature are shown in Figure. 3.4b. The decay curve at 10 K is slightly nonexponential which seems to be due to the existence of two decay components. The anomalous decay phenomenon is also reported in self-activated

NaWO₂PO₄ phosphor by Blasse et al. The average decay time can be calculated by the following equation:

$$\tau_{\text{avg}} = \frac{\int tI(t)dt}{\int I(t)dt} \quad (3.2)$$

The measured luminescence decay time is shortened significantly in the elevated temperature region and the decay kinetics of the emitting WO₅Cl group exhibit a singular exponential decay. The average decay times reduce from 222.9 μs at 10 K to 48.4 μs at 420 K for Ca₃WO₅Cl₂, due to the nonradiative transition probability at a low temperature is lower than that at a higher temperature.

The average decay time as a function of temperature is revealed in Figure. 3.4(c). The results could be explained by a three-level scheme [58, 59, 62] as illustrated in Figure. 3.4(d), where level 1 is the singlet ground state, level 2 is a metastable excited level and level 3 belongs to an excited triplet level with the energy separation \mathcal{E} between levels 2 and 3. p_{23} and p_{32} are nonradiative relaxation rates between levels 2 and 3. It is assumed that one photon is excited from the ground state to the lower excited state 2 and then trapped thermally by the de-excited state 3 resulting in the emission with the radiative transition p_{31} , while p_{21} is an unobserved transition, which could be supposed as a non-radiative process. The thermal quenching rate p_Q from level 2 to level 1 are considered in a uniform form. Therefore, the luminescence decay time depending on temperature is given by the following equation [56-58]:

$$\tau^{-1}(T) = p_{31} \left[1 + \exp\left(\frac{\mathcal{E}}{kT}\right) \right]^{-1} + p_{21} \left[1 + \exp\left(-\frac{\mathcal{E}}{kT}\right) \right]^{-1} + w_1 \exp\left(-\frac{E}{kT}\right) \quad (3.1)$$

Where \mathcal{E} is the energy separation between level 2 and level 3, w_1 is frequency factor, E is the activation energy, and k is the Boltzmann constant. The experimental decay times are well fitted to eq. (2) as shown in Figure. 3.4c and the fitting results are as follows: $p_{21} = 20723 \text{ s}^{-1}$, $p_{31} = 82623 \text{ s}^{-1}$, $\mathcal{E} = 1828 \text{ cm}^{-1}$, $w_1 = 1.28 \times 10^8 \text{ s}^{-1}$, and $E = 1828 \text{ cm}^{-1}$. The values of calculated parameters and comparative data from other system are listed in Table 3.

Table 3.3 The doping concentration of Eu³⁺ ions dependent CIE values of Ca₃WO₅Cl₂:Eu³⁺

Compound	CIE (\bar{x})	CIE (\bar{x})
$\text{Ca}_3\text{WO}_5\text{Cl}_2$	0.2017	0.2600
$\text{Ca}_3\text{WO}_5\text{Cl}_2:0.1\text{mol}\%$	0.2017	0.2600
$\text{Ca}_3\text{WO}_5\text{Cl}_2:1.0\text{mol}\%$	0.2035	0.2596
$\text{Ca}_3\text{WO}_5\text{Cl}_2:3.0\text{mol}\%$	0.2058	0.2572
$\text{Ca}_3\text{WO}_5\text{Cl}_2:5.0\text{mol}\%$	0.2221	0.2616
$\text{Ca}_3\text{WO}_5\text{Cl}_2:7.0\text{mol}\%$	0.2351	0.2616
$\text{Ca}_3\text{WO}_5\text{Cl}_2:9.0\text{mol}\%$	0.2649	0.2613

3.2.3 Luminescent performance of $\text{Ca}_3\text{WO}_5\text{Cl}_2:\text{Eu}^{3+}$

The XRD measurements for Eu^{3+} -doped samples verified that the maximum tolerable doping level of Eu^{3+} ions in $\text{Ca}_3\text{WO}_5\text{Cl}_2$ lattices is about 9 mol % (Figure. 3.5). The impurity phases could be detected when the doping contain excesses 9 mol% due to the different ions' radius and the charge balance between the Eu^{3+} ions (1.066 Å, CN=8) and the substituted Ca^{2+} ions (1.12 Å, CN=8) [63].

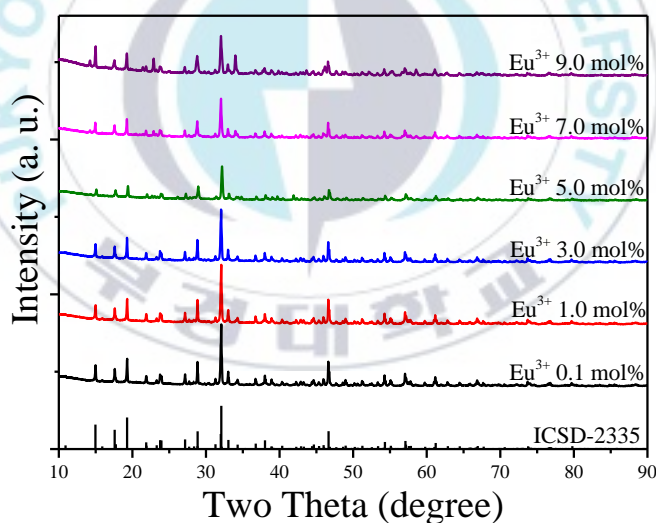


Figure 3.5 XRD patterns of $\text{Ca}_3\text{WO}_5\text{Cl}_2:\text{Eu}^{3+}$ phosphors with different Eu^{3+} doping concentration along with the ICSD card (ICSD-2335).

Surface morphology of phosphors was investigated by SEM, Figure. 3.6 shows the SEM images of 3 mol% Eu^{3+} ions doped $\text{Ca}_3\text{WO}_5\text{Cl}_2$ phosphors with the size distribution in the range of 2 μm and 1 μm . The particles of the samples are mostly irregular layered shapes, and all samples have in the phenomenon of agglomeration.

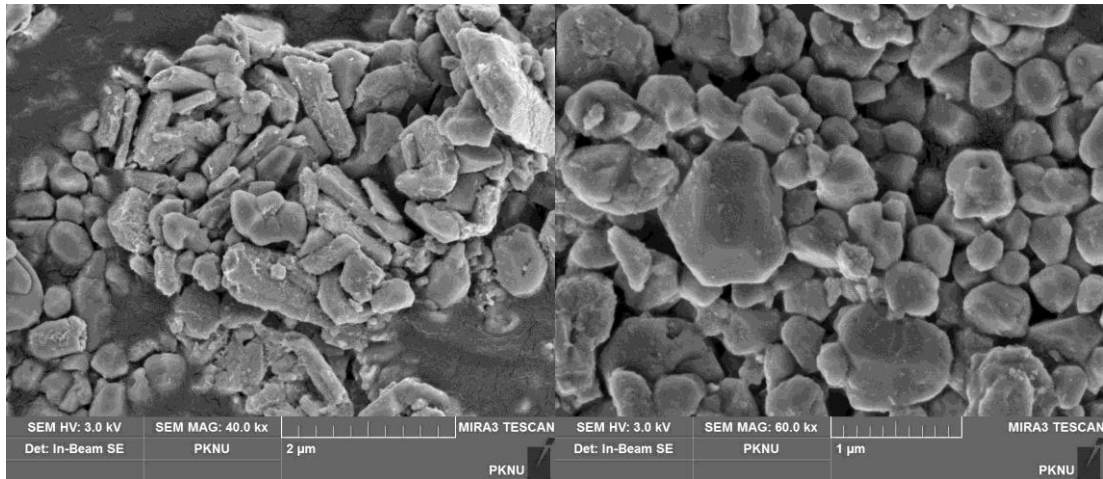


Figure 3.6 SEM images of 3 mol% Eu^{3+} ions doped $\text{Ca}_3\text{WO}_5\text{Cl}_2$ phosphors.

Figure 3.7 represents the PLE spectra of Eu^{3+} ions doped $\text{Ca}_3\text{WO}_5\text{Cl}_2$ phosphors obtained by monitoring the 615 nm emission correspond to the $^5\text{D}_0 \rightarrow ^7\text{F}_2$ transition at room temperature. The PLE spectra can be separated into two parts, one is a broadband ranging from 200 to 350 nm with a maximum in the wavelength of about 340 nm, which corresponding to the charge transfer band (CTB) from the 2p orbital of the O^{2-} ligand to the 4f orbital Eu^{3+} and the 5d orbital of the d^0 tungsten metal ion. The other part is a series of sharp excitation peaks in the wavelength region from 350 to 450 nm corresponding to the 4f-4f transitions ($^7\text{F}_0 \rightarrow ^5\text{D}_{0,1,2,3,4,5}\text{L}_{6,7}, ^5\text{H}_3$) of Eu^{3+} ions. The most intense line is observed at 394 nm due to the $^7\text{F}_0 \rightarrow ^5\text{L}_6$ transition. This means that near-ultraviolet LED chips (around 400 nm) the phosphor can be efficiently excited.

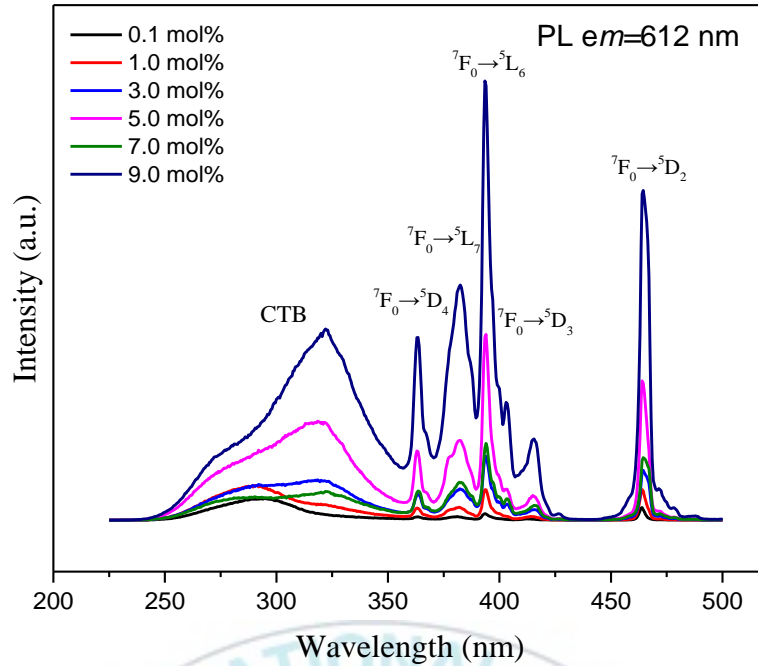


Figure 3.7 The room temperature excitation spectra of $\text{Ca}_3\text{WO}_5\text{Cl}_2:\text{xEu}^{3+}$ ($x = 0.1, 1.0, 3.0, 5.0, 7.0$ and 9.0 %) phosphors.

The Eu^{3+} ions concentration dependent emission spectra of $\text{Ca}_3\text{WO}_5\text{Cl}_2:\text{Eu}^{3+}$ were obtained by excitation with 266 nm radiation at room temperature as shown in Figure. 3.8(a). The characteristic emission peaks of Eu^{3+} ions can be observed in the red emission region at around 615 nm together with the host emission band in the blue emission region at around 450 nm. Accordingly, the band at 450 nm originates from charge transfer behavior of WO_5Cl group, while the sharp lines at 615 nm originates from the ${}^5\text{D}_0$ - ${}^7\text{F}_j$ transitions of Eu^{3+} ions. As the Eu^{3+} concentration increases, the luminescence intensity of the Eu^{3+} ions increase, while that of the WO_5Cl group band decreases rapidly (Figure. 3.8(b)).

The energy transfer efficiency η_T can be approximately calculated by the following equation [64]:

$$\eta_T = 1 - \frac{I_{s0}}{I_s} \quad (3.4)$$

where η_T represents the energy transfer efficiency, I_{s0} and I_s represent the luminescence intensity of tungstate group in the absence and presence of Eu^{3+} ions. Figure. 8c shows the calculated transfer efficiency in $\text{Ca}_3\text{WO}_5\text{Cl}_2:\text{Eu}^{3+}$ phosphors. The energy transfer efficiency η_T increase monotonously and reaches the maximum value of 40% at $x = 9.0$ mol%.

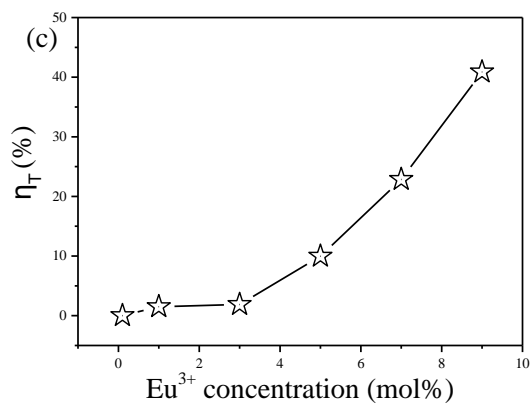
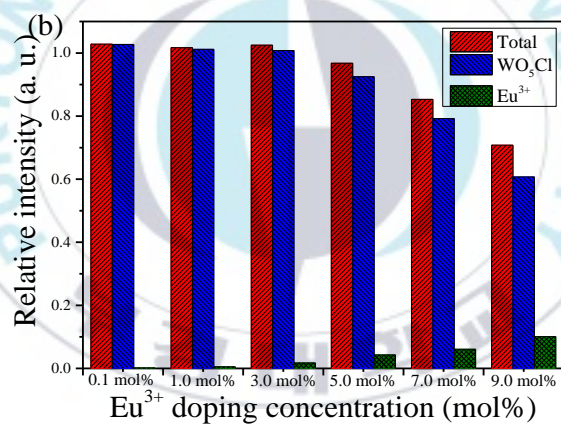
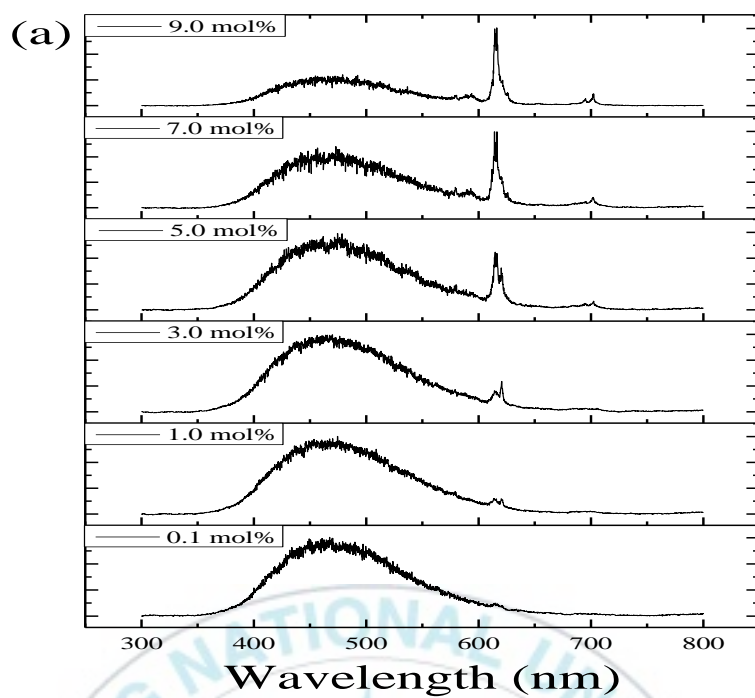
According to the Dexter's energy transfer formula of multipolar interaction and Reisfeld's approximation, the relationship between WO_5Cl group and Eu^{3+} ions can be obtained by the following equation [65, 66]:

$$\frac{\eta_{s0}}{\eta_s} \propto C^{n/3} \quad (3.5)$$

where η_{s0}/η_s represents the ratio of luminescence quantum efficiencies of the WO_5Cl group in the absence and presence of Eu^{3+} ions, C represents the doping concentration of the Eu^{3+} ions, and $n = 6, 8$ and 10 represent electric dipole-dipole (d-d), dipole-quadrupole (d-p), and quadrupole-quadrupole (q-q) interactions, respectively [67]. Here, the ratio of luminescence quantum efficiencies of $\eta_{s0}=\eta_s$ can be approximately estimated by the luminescence intensity ratio of $I_{s0}=I_s$.

The pattern in Figure. 3.8(d) shows the plots of I_{s0}/I_s vs $C^{n/3}$. As shown in the pattern, based on the value of R^2 , the best linear behavior is observed when $n = 10$, indicating that the energy transfer occurs through the d-p interaction mechanism. In conclusion, in the $\text{Ca}_3\text{WO}_5\text{Cl}_2$ lattice, the energy transfer behavior from WO_5Cl group to Eu^{3+} ions occur through the q-q interaction mechanism.

Significantly, the emissions from host WO_5Cl octahedral are always exist even in Eu^{3+} -condensed $\text{Ca}_3\text{WO}_5\text{Cl}_2$ halotungstates. It is well known that some compounds containing MO_x group (M is a high valence d^0 ion), such as vanadates, molybdates, tungstates, the energy transfer occurs via either an exchange or super exchange mechanism, and is depended on the M-O-RE bond angle in the host lattices [68-70]. For example, M-O-RE bond angle of 180° would maximize wave-function overlap and the energy transfer efficiency.



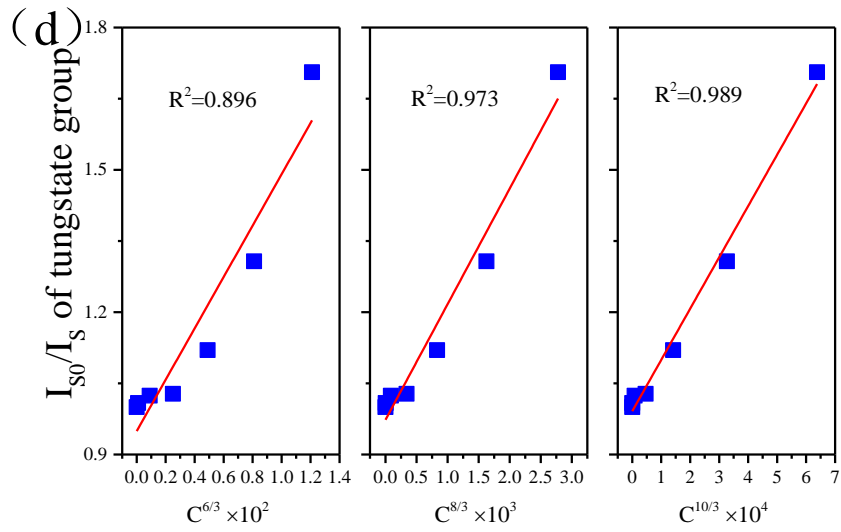


Figure 3.8 (a) The room temperature concentration-dependent emission spectra of $\text{Ca}_3\text{WO}_5\text{Cl}_2:\text{Eu}^{3+}$ ($x = 0.1, 1.0, 3.0, 5.0, 7.0$ and 9.0 %). (b) Relative intensity of Eu^{3+} . (c) energy transfer efficiency η_T with different doping concentration (d) the plots of I_{S0}/I_S vs $C^{n/3}$.

Figure 3.9 shows the schematic view of the coordination geometries around the Eu1 (a), Eu2 (a) and Eu3 (a) polyhedrons in $\text{Ca}_3\text{WO}_5\text{Cl}_2:\text{Eu}^{3+}$ phosphors. The W-O/Cl-Eu bond angle is about 102° and 139° for Eu1, 60° , 102° and 139° for Eu2, 63° , 104° , 135° and 162° for Eu3 in $\text{Ca}_3\text{WO}_5\text{Cl}_2:\text{Eu}^{3+}$ phosphors, which reduces somewhat wave-function overlap and the exchange energy transfer efficiency. Consequently, the emission from WO_5Cl group in $\text{Ca}_3\text{WO}_5\text{Cl}_2$ halotungstates can be still observed [71].

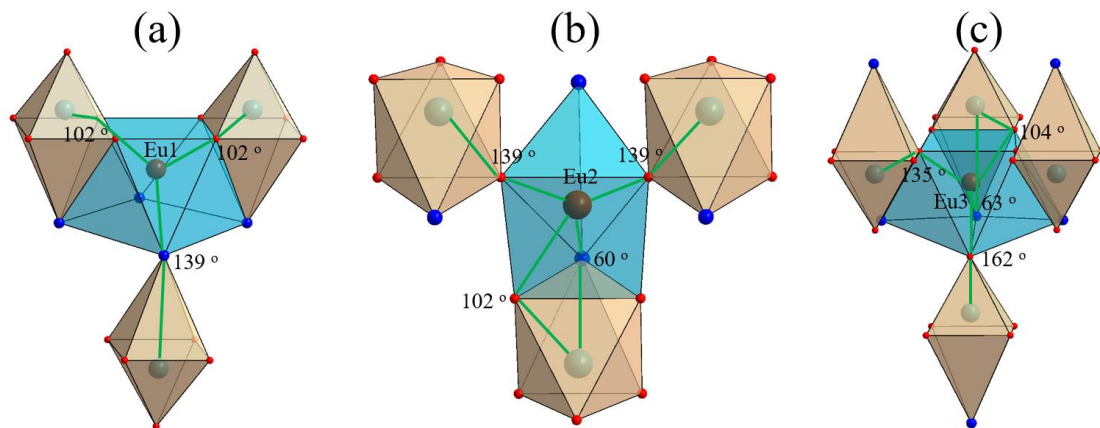


Figure 3.9 The schematic view of the coordination geometries around the Eu1 (a), Eu2 (a) and Eu3 (a) polyhedrons.

The decay curves of the concentration dependent Eu^{3+} doping $\text{Ca}_3\text{WO}_5\text{Cl}_2$ excited by 266 nm and monitored by 615 nm at temperature are shown in Figure. 3.10. The decay curve of $\text{Ca}_3\text{WO}_5\text{Cl}_2: x\text{Eu}^{3+}$ overlapped very well when Eu^{3+} changed, which implied that the luminescence of Eu^{3+} did not quenched with increasing concentration. The decay curves can be fitted by a single-exponential decay model.

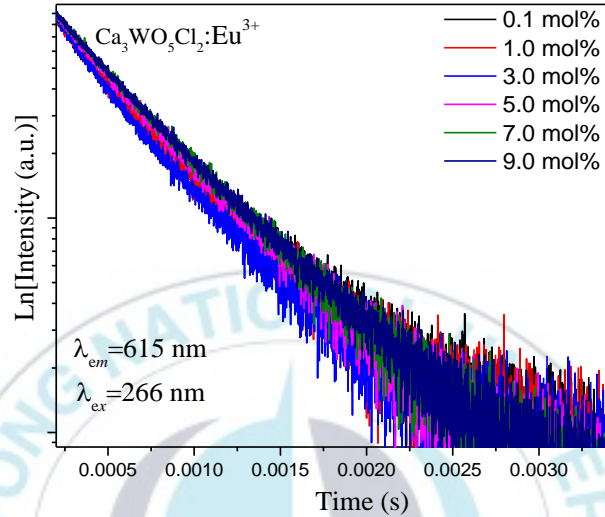


Figure 3.10 The decay curves of the $\text{Ca}_3\text{WO}_5\text{Cl}_2:\text{Eu}^{3+}$ phosphors with different Eu^{3+} doping concentration.

To evaluate the colorimetric performance of the prepared phosphors, the Commission Internationale de l'Éclairage(CIE) 1931 chromaticity coordinates for $\text{Ca}_3\text{WO}_5\text{Cl}_2$ phosphors doped with different Eu^{3+} concentration and excited at 266 nm are calculated using the intensity corrected emission spectra. Upon excitation with 266 nm, the emitted light changes its color from a blue green to a white as the doping concentration is increased. At the doping level of 0 mol% and 9 mol%, the CIE coordinates are $x = 0.2617$ and $y = 0.26$; and $x = 0.2681$ and $y = 0.2638$ respectively. This indicates a red shift with increasing concentration of dopant (Eu^{3+}).

The CIE color coordinates diagram is shown in Figure. 3.11 [72].

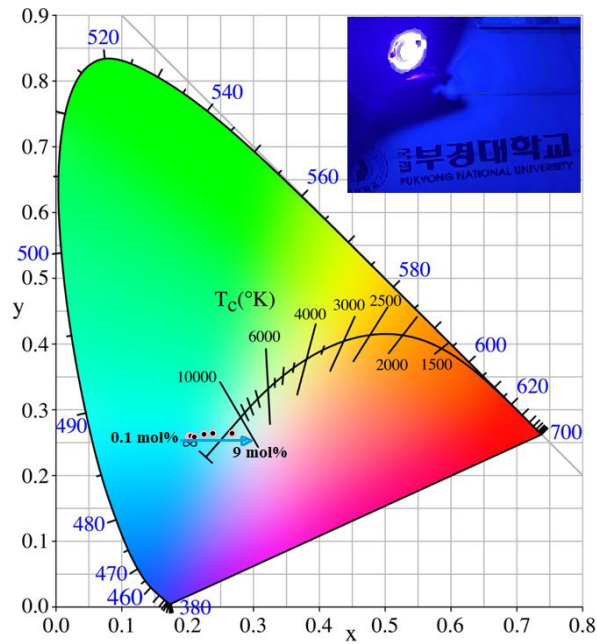


Figure 3.11 The CIE and led chips of $\text{Ca}_3\text{WO}_5\text{Cl}_2$ phosphors.

The energy transfer process from the WO_5Cl group to Eu^{3+} in $\text{Ca}_3\text{WO}_5\text{Cl}_2$ phosphors shown in Figure. 3.12. Under excitation at 266 nm, the electrons get excited to WO_5Cl group and by non-radiative transitions these electrons relax to lower energy states and then by transferring their energies they excite Eu^{3+} ions to higher energy states ($^5\text{D}_0$). These excited Eu^{3+} ions return to the ground states of Eu^{3+} ($^7\text{F}_2$) by radiative transition in red region.

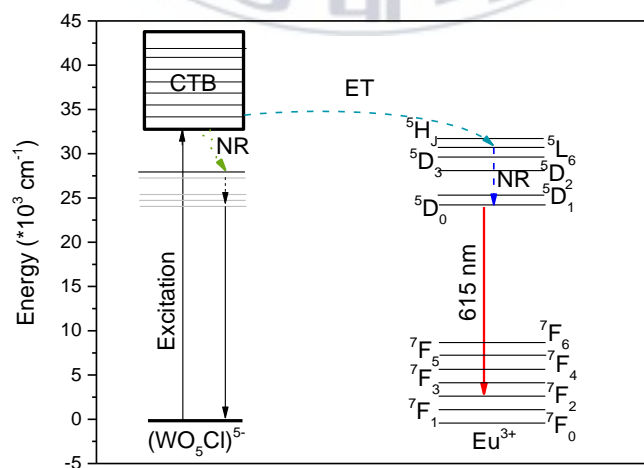


Figure 3.12 Schematic energy level diagram for transfer process between WO_5Cl group and Eu^{3+} ions in $\text{Ca}_3\text{WO}_5\text{Cl}_2$ phosphors.

3.2.4 High-temperature luminescence of $\text{Ca}_3\text{WO}_5\text{Cl}_2:\text{Eu}^{3+}$

To further study the emission thermal stability and potential application in LEDs, the emission spectra and decay curves of the $\text{Ca}_3\text{WO}_5\text{Cl}_2:\text{Eu}^{3+}$ (5 mol %) phosphor are studied in the temperature region of 300 - 480 K under excitation at 266 nm. In Figure. 3.11(a) displays with increasing temperature, the spectral shape and peaks unchanged and both the emission intensity for WO_5Cl group and ${}^5\text{D}_0\text{-}{}^7\text{F}_j$ transitions of Eu^{3+} ions decrease. Which is beneficial to prepare stable luminescence at elevated temperature. The luminescence normalized integrated intensities of $\text{Ca}_3\text{WO}_5\text{Cl}_2:\text{Eu}^{3+}$ (5 mol %) phosphors in the temperature region 300-480 K are shown in Figure. 3.11(a), the intensity of the $\text{Ca}_3\text{WO}_5\text{Cl}_2:\text{Eu}^{3+}$ (5 mol %) phosphors becomes weak with an increasing temperature 300 K to 480 K, owing to the thermal quenching effect [73].

In general, the thermal quenching performance of phosphors is usually investigated based on activation energy of materials. Activation energy of materials is calculated by following equation as [74]:

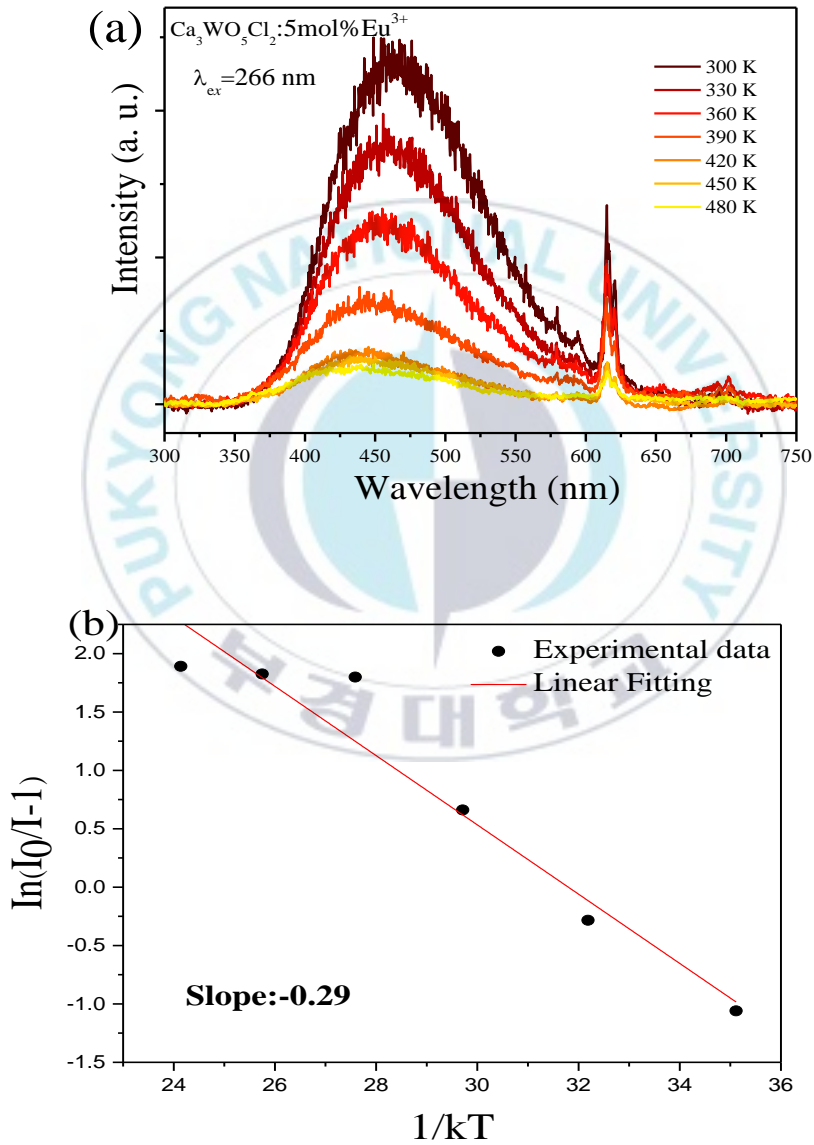
$$I(T) = \frac{I_0}{1 + c \exp(-E_a/kT)} \quad (3.5)$$

Where I_0 represents emission intensity of the phosphors at room-temperature, $I(T)$ is emission intensity at different temperatures, c is a constant for a certain host, E_a is the activation energy and k is the Boltzmann constant (8.63×10^{-5} eV).

Figure. 3.10(b) presents the plot of $\ln I_0/I - 1$ vs. $1/kT$. The experimental data can be fitted linearly. The slope is -0.29 , so the activation energy for the thermal quenching is 0.29 eV. The value is similar to those of the reported red phosphor such as $\text{Y}_2\text{MoSiO}_8:\text{Eu}^{3+}$ [75], $\text{Ca}_2\text{MgTeO}_6:\text{Eu}^{3+}$ [76], $\text{BiLaWO}_6:\text{Eu}^{3+}$ [77], $\text{Ba}_3\text{Y}_4\text{O}_9:\text{Eu}^{3+}$ [26]. The high ΔE proved the $\text{Ca}_3\text{WO}_5\text{Cl}_2:\text{Eu}^{3+}$ (5 mol %) phosphors had good thermal stability.

Thermal stability is often important for phosphors, as it is well known that as the temperature increases, the luminescence intensity becomes weaker, and accordingly, the luminescence lifetime τ becomes shorter. It has been demonstrated that the transition probability is proportional to τ^{-1} . In order to explore the thermal stability of $\text{Ca}_3\text{WO}_5\text{Cl}_2:\text{Eu}^{3+}$ (5 mol %) luminescence, the luminescence decay lifetime of the phosphor at 300-480 K was

measured. The temperature-dependent decay curves of the $\text{Ca}_3\text{WO}_5\text{Cl}_2:\text{Eu}^{3+}$ (5 mol %) phosphor by monitoring 615 nm emission under 266 nm excitation were recorded from 300 K to 480 K, as shown in Figure. 3.11(c). The calculated values of decay time for $\text{Ca}_3\text{WO}_5\text{Cl}_2:\text{Eu}^{3+}$ (5 mol %) phosphor shown in Figure. 3.11(d), decreases from 0.53 ms to 0.42 ms with the increase of environment temperature 300 K to 480 K, mirroring the increase of probability of non-radiative transition at elevated temperature [78].



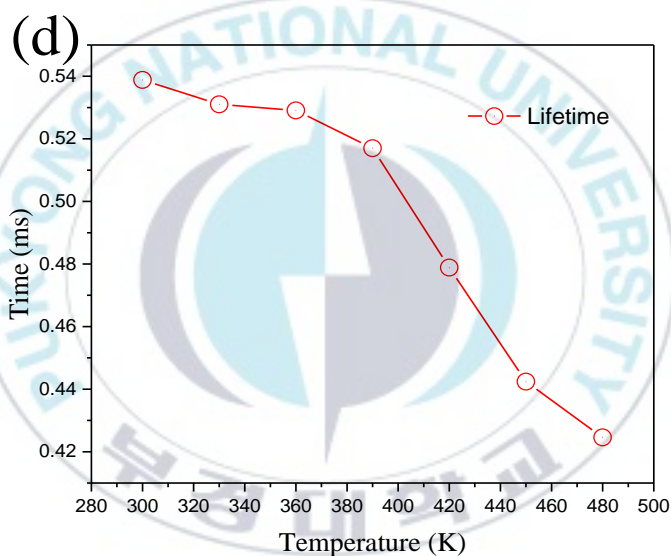
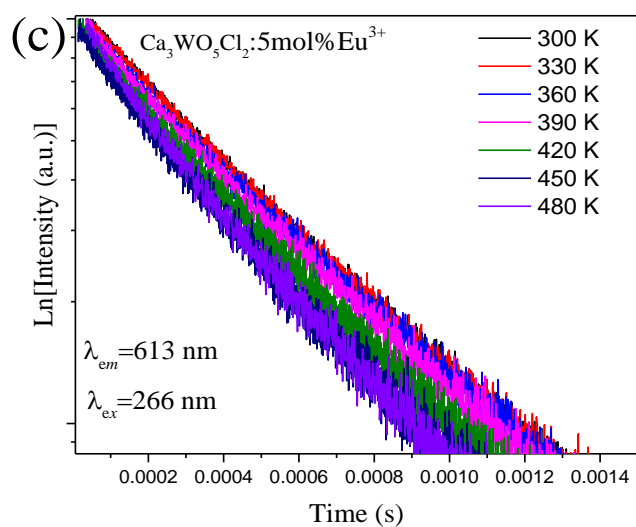


Figure 3.13 (a) The temperature dependent emission spectra of $\text{Ca}_3\text{WO}_5\text{Cl}_2:\text{Eu}^{3+}$ (5 mol%) phosphors. (b) The relationship of $\ln[(I_0/I) - 1]$ vs. $1/kT$ activation energy graph for thermal quenching of the $\text{Ca}_3\text{WO}_5\text{Cl}_2:\text{Eu}^{3+}$ (5 mol%) phosphors. (c) The temperature dependent decay curves of $\text{Ca}_3\text{WO}_5\text{Cl}_2:\text{Eu}^{3+}$ (5 mol%) phosphors. (d) The calculated lifetime of $\text{Ca}_3\text{WO}_5\text{Cl}_2:\text{Eu}^{3+}$ (5 mol%) phosphors with increasing temperature.

The Commission Internationale de l'Éclairage (CIE) 1931 chromaticity coordinates for $\text{Ca}_3\text{WO}_5\text{Cl}_2:\text{Eu}^{3+}$ (5 mol %) phosphor with different temperature excited at 266 nm and CIE coordinates can be used to calculate correlated color temperature CCT, both calculated in Table 3.4. The CIE coordinate value of self-activated $\text{Ca}_3\text{WO}_5\text{Cl}_2$ phosphor located on blue region, CIE coordinates of $\text{Ca}_3\text{WO}_5\text{Cl}_2:\text{Eu}^{3+}$ (5 mol %) phosphor at different temperature are similar with CIE coordinate of self-activated $\text{Ca}_3\text{WO}_5\text{Cl}_2$ phosphor. These results showing that the

material can be used in clinical applications and blue LEDs. This improvement managed to the displays for iPads, cell phones, computers, TVs, etc [76, 79].

Table 3.4 The temperature dependent CIE values of $\text{Ca}_3\text{WO}_5\text{Cl}_2:5\text{mol}\%\text{Eu}^{3+}$.

Temp. (K)	CIE (x)	CIE (y)	CCT
300	0.21160	0.25057	29735
330	0.2086876	0.2364189	49862
360	0.2238327	0.2310688	46317
390	0.2361424	0.2327774	38162
420	0.2219857	0.2141462	112863
450	0.2312386	0.2214883	63587
480	0.2462275	0.2241072	43873

3.3 Conclusion

The $\text{Ca}_3\text{WO}_5\text{Cl}_2$ and $\text{Ca}_3\text{WO}_5\text{Cl}_2: \text{Eu}^{3+}$ were synthesized via the facile solid-state reactions. Under UV-light, the $\text{Ca}_3\text{WO}_5\text{Cl}_2$ phosphor shows typical self-activated luminescence from the allowed charge transfer transitions in $[\text{WO}_5\text{Cl}]^{5-}$ groups. The temperature-dependent (10–480 K) luminescence of $\text{Ca}_3\text{WO}_5\text{Cl}_2$ shows with the increasing temperature from 10 to 480 K, the emission intensity decreases. The decay curves of the $\text{Ca}_3\text{WO}_5\text{Cl}_2$ are shorter than other self-activated tungstate materials. Eu^{3+} activated tungstate shows energy transfer from $[\text{WO}_5\text{Cl}]^{5-}$ groups to Eu^{3+} ions have been observed during the photoluminescence of the Eu^{3+} -doped compounds. The emission intensity relating to $[\text{WO}_5\text{Cl}]^{5-}$ groups decreases with increasing Eu^{3+} concentration. The emission intensity of $\text{Ca}_3\text{WO}_5\text{Cl}_2 \text{Eu}^{3+}$ (5 mol %) phosphor decreases with increasing temperature and the lifetime of the $\text{Ca}_3\text{WO}_5\text{Cl}_2 \text{Eu}^{3+}$ (5 mol %) phosphor do not change significantly with the increasing temperature. And the obtained $\text{Ca}_3\text{WO}_5\text{Cl}_2 \text{Eu}^{3+}$ (5 mol %) phosphor possesses good thermal stability, having potential application in white light diodes (WLEDs).

4. Photoluminescence properties of red-emitting Mn²⁺-activated Na₂Mg(PO₃)₄ phosphors for white-LEDs

4.1 Introduction

Recently, white-LED (Light Emitting Diode) with energy saving and low-cost characteristics have attracted worldwide attention. Rare earth (RE) ions, especially for the ions with 5d → 4f or 4f → 4f transitions, play an important role in display and modern lighting fields owing to their abundant emission colors [64, 80, 81]. However, it is well known that the reserves of RE elements on earth are limited, which usually leading to the high prices for phosphors using RE ions as luminescence centers. Therefore, recently, non-RE ions doped phosphors have attracted extensive attention, for example the phosphors doped with Cr³⁺, Mn²⁺ or Mn⁴⁺. Among these non-RE ions, as an alternative, the phosphors doped with Mn²⁺ provide some important advantages in this respect and thus have attracted more and more attention recently.

Mn²⁺ as a transition metal ion, the outer electron configuration 3d⁵ which will be strongly effected by the crystal field of the host lattice. Under the action of excitation energy, the electrons in Mn²⁺ ions will be excited from the ground state ⁶A₁(⁶S) level of Mn²⁺ to the higher excited state (such as ⁴E(⁴D), ⁴E(⁴G), ⁴T₁(⁴P), ⁴T₂(⁴D), and ⁴A₁(⁴G)) levels in the UV to blue region (300-480 nm), then relax to the lowest excited state of ⁴T₁(⁴G) with non-radiation process. Finally, the forbidden transition ⁴T₁(⁴G) → ⁶A₁(⁶S) produced with a broad band transmission [82]. With the increase of crystal field strength, the energy level splitting increases resulting in the lowest energy level ⁴T₁(⁴G) moves down, and then the emission wavelength redshifts, even reaches the near-infrared region. Conversely, the crystal field splitting decreases, and the lowest energy level ⁴T₁(⁴G) will moves up, and then the emission wavelength blueshifts, even reaches the green region [83]. Accordingly, J. A. Hodges point out that Mn²⁺ ions can enter the tetra-coordination, hexa-coordinate and octa-coordinate in some lattice in order to increase the absorption efficiency of phosphors, it is natural and effective to increase Mn concentration due

to the fact that phosphors doped with high concentration of Mn^{2+} without causing serious concentration quenching. The non-concentration quenching phenomenon can be expected to have high absorption efficiency for the excitation light, and consequently, high PL output.

In this work, $\text{Na}_2\text{Mg}(\text{PO}_3)_4$ host was selected to explore a novel Mn^{2+} activated red-emitting phosphor for W-LED. The excitation wavelength in the region from 300 to 500 nm matches well with the characteristic emission of UV LED chips. The experiment characterization methods such as XRD, PL, PLE spectra and luminescence decay were employed in order to investigate the optical performance. Otherwise, the thermal stability was analyzed, which are attractive characteristics for white LED applications and discuss characteristics.

4.2 Results

4.2.1 Crystal structural refinement

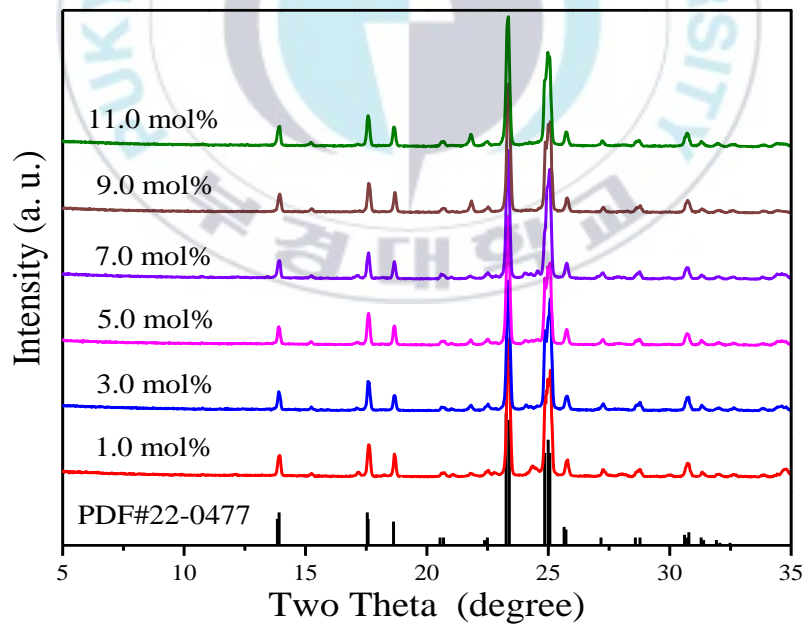


Figure 4.1 XRD patterns of $\text{Na}_2\text{Mg}_{1-x}(\text{PO}_3)_4:x\text{Mn}^{2+}$ phosphors with different Mn^{2+} doping concentration sintered at 850 °C for 6 h, along with the standard PDF card (PDF#22-0477).

Figure. 4.1 exhibits the XRD patterns of $\text{Na}_2\text{Mg}_{1-x}(\text{PO}_3)_4:x\text{Mn}^{2+}$ with different doping contents of Mn^{2+} ions and compared with the standard PDF card. Due to the similar ions radii

and the same valance state, it is suggested that the Mg^{2+} ions will be replaced by Mn^{2+} ions. All the XRD patterns are in good agreement with the standard PDF card #22-0477 and there are no trace of impurity phase can be detected, suggesting that as-synthesized phosphors are confirmed to be single-phase, and the doping of the Mn^{2+} ions does not cause any significant changes in $\text{Na}_2\text{Mg}(\text{PO}_3)_4$ lattice.

4.2.2 Optical performances

The luminescence mechanism of Mn^{2+} ions usually can be described by the Tanabe-Sugano energy level diagram of d^5 configuration as exhibited in Figure. 4.2(a). The horizontal axis presents the Dq/B values to evaluate crystal field strength, while the vertical axis represents the energy levels of the free Mn^{2+} ion and the energy levels of the crystal field splitting acting on the Mn^{2+} ion. As the diagram shows, the luminescent properties of Mn^{2+} are strongly dependent on the crystal field where Mn^{2+} ions locate. Generally, when Mn^{2+} ions replace the tetrahedral positions with relatively weak crystal field, the phosphors emit green emission, conversely, when Mn^{2+} ions replace the octahedral positions, the phosphors emit orange to red emission [84].

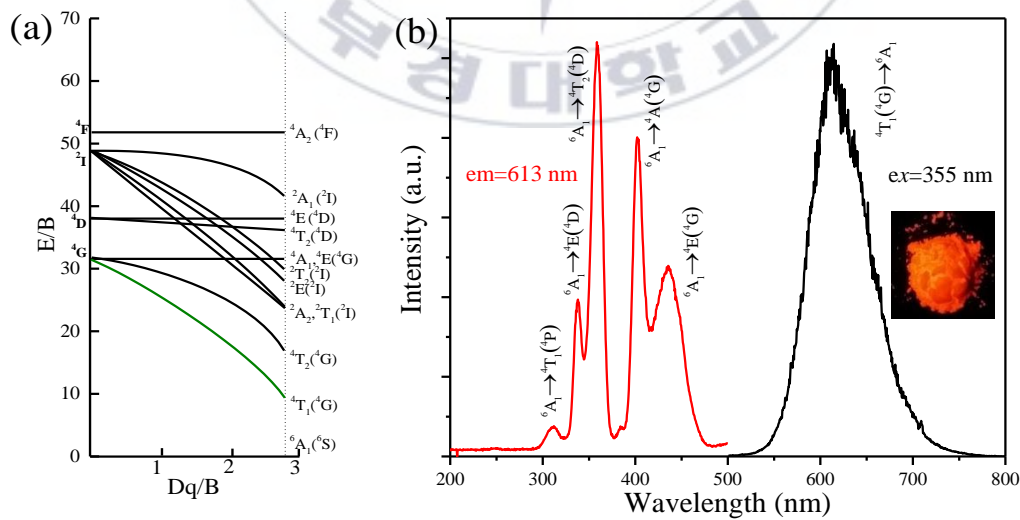


Figure 4.2. (a) The energy-level diagram of Mn^{2+} ions, (b) PL and PLE spectra of the typical Mn^{2+} ions doped in $\text{Na}_2\text{Mg}(\text{PO}_3)_4$ lattice.

Figure 4.2(b) shows typical excitation and emission spectra of the $\text{Na}_2\text{Mg}(\text{PO}_3)_4:\text{Mn}^{2+}$ red phosphor. The emission spectrum was obtained under excitation at 355 nm and the excitation spectrum was detected by monitoring the 613 nm emission. As figure shows, the PL spectrum is composed of five bands, which cover the spectral range 250 - 550 nm. They are assigned to the transitions from the ground state ${}^6\text{A}_1(\text{S})$ to the ${}^4\text{E}({}^4\text{D})$, ${}^4\text{E}({}^4\text{G})$, ${}^4\text{T}_1({}^4\text{P})$, ${}^4\text{T}_2({}^4\text{D})$, and ${}^4\text{A}_1({}^4\text{G})$ states, respectively. The most intense excitation bands at 360 and 410 nm correspond to the ${}^6\text{A}_1(\text{S}) \rightarrow {}^4\text{T}_2({}^4\text{G})$, ${}^4\text{A}_1({}^4\text{G})$ transitions, indicating that the $\text{Na}_2\text{Mg}(\text{PO}_3)_4:\text{Mn}^{2+}$ red phosphors can be stimulated by UV, near UV and blue light. The PL spectrum shows a broad band emission peaking at 613 nm, which can be ascribed to the spin-forbidden ${}^4\text{T}_1({}^4\text{G}) \rightarrow {}^6\text{A}_1$ transition. The red emission indicated that all the Mn^{2+} ions are coordinated by six O^{2-} ions forming octahedral sites [85-87].

The colorimetric properties were introduced to evaluate the luminescence properties of $\text{Na}_2\text{Mg}(\text{PO}_3)_4:9\%\text{Mn}^{2+}$. By using the CIE 1938 system, the CIE index were calculated as ($x=0.628$, $y=0.371$) according to the PL spectrum. From Figure 4.2(b), it can be seen that the CIE coordinates measured for the $\text{Na}_2\text{Mg}(\text{PO}_3)_4:9\%\text{Mn}^{2+}$ phosphor are falling on the red region which is in consonance with the PL spectrum shown in Figure 4.2(b). At the same time, the digital photo of the $\text{Na}_2\text{Mg}(\text{PO}_3)_4:9\%\text{Mn}^{2+}$ phosphor is shown as well under a 355 nm UV lamp. Besides, the color purity (CP) of the phosphor can be determined according to the equation as following:

$$\text{Color purity} = \frac{\sqrt{(x-x_i)^2 + (y-y_i)^2}}{\sqrt{(x_d-x_i)^2 + (y_d-y_i)^2}} \quad (4.1)$$

where the (x , y) refer to the color coordinates of the $\text{Na}_2\text{Mg}(\text{PO}_3)_4:9\%\text{Mn}^{2+}$ phosphor with the values of ($x=0.628$, $y=0.371$) under the excitation of 355 nm. The white illuminant point (x_i , y_i) and the dominated wavelength point (x_d , y_d) were equal to (0.310, 0.316) and (0.675, 0.325), respectively. According to the Eq. (1), the color purity of the $\text{Na}_2\text{Mg}(\text{PO}_3)_4:9\%\text{Mn}^{2+}$ phosphor can be calculated to be 88.4%, which further indicates that the synthesized phosphor has a high color purity and has a promising application prospect in near UV to blue light excited W-LEDs.

The correlated colour temperature (CCT) is another important tool to evaluate the luminescence properties of $\text{Na}_2\text{Mg}(\text{PO}_3)_4:9\%\text{Mn}^{2+}$, which can be estimated using the following formula proposed by McCamy:

$$\text{CCT} = -449n^3 + 3525n^2 - 6823.2n + 5520.3 \quad (4.2)$$

where $(x-x_e)/(y-y_e) = n$ refers to the inverse slope line, where $x_e = 0.332$ and $y_e = 0.186$ refer to the epicenter of the convergence. From Eq. (4.2), the value of CCT for the $\text{Na}_2\text{Mg}(\text{PO}_3)_4:9\%\text{Mn}^{2+}$ phosphor was calculated to be 1788 K. Generally, the phosphors with the $\text{CCT} < 5000$ K can be used for warm white light, and other phosphor with the $\text{CCT} > 5000$ K can be used for cold white light. The calculated CCT value for the $\text{Na}_2\text{Mg}(\text{PO}_3)_4:9\%\text{Mn}^{2+}$ phosphor was noticed to be < 5000 K indicating that it can be served as the warm-white LEDs applications.

4.2.3 Concentration-dependent luminescence properties of Mn^{2+} -doped $\text{Na}_2\text{Mg}(\text{PO}_3)_4$

Figure. 4.3(a) shows Mn^{2+} concentration dependent emission spectra under the excitation of 355 nm at room temperature. When Mn^{2+} concentration increases from 1.0 mol % to 9.0 mol %, the emission intensity increases. For all samples, the profile of PL spectra are nearly the same except for the intensity, and the optimum concentration of Mn^{2+} ion for $\text{Na}_2\text{Mg}(\text{PO}_3)_4$ system is 9 mol%. For further increase in Mn^{2+} concentration up to 11 mol% the quenching of the emission begins to occur. Based on isotropic exchange interaction between Mn^{2+} ions, the formation of Mn^{2+} ion pairs and clusters were revealed to be the leading factor of concentration quenching behavior [88, 89]. Figure. 4.3(b) indicates the calculated emission intensities of various doping concentration of Mn^{2+} ions in $\text{Na}_2\text{Mg}(\text{PO}_3)_4$ lattice. As figure shows, the excitation intensity increased firstly and then decreased which can be ascribed to the concentration quenching behavior. According to Dexter theory, non-radiative transitions between Mn^{2+} ions should be controlled by multipole electrical interactions, which can be ascribed to the allowed electric dipole transitions. And the type of interaction can usually be determined by the equation as following equation:

$$\frac{I}{x} = \frac{k}{1 + \beta(x)^{\theta/3}} \quad (4.3)$$

where x refers to the doping concentration of Mn^{2+} ions, I represents the PL intensity, k and β represent the constants. The interaction type of nonradiative transitions can be denoted by the value θ , where $\theta = 3, 6, 8,$ and 10 , refer to the nonradiative transitions between nearest Mn^{2+} ions, electric dipole-dipole, dipole-quadrupole, and quadrupole-quadrupole interactions, respectively. Here in this work, as shown in the illustration of Figure. 4.3(b), the θ obtained by linear fitting method was 2.62 on the basis of the relationship between $\log x$ and $\log I/x$. The fitting result indicate that the dominant concentration quenching behavior is realized by the nonradiative transitions between nearest Mn^{2+} ions.

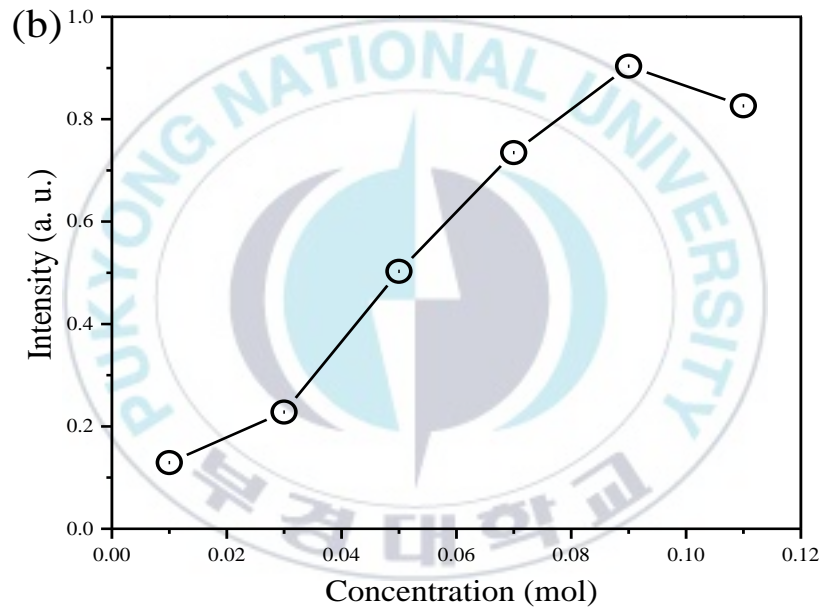
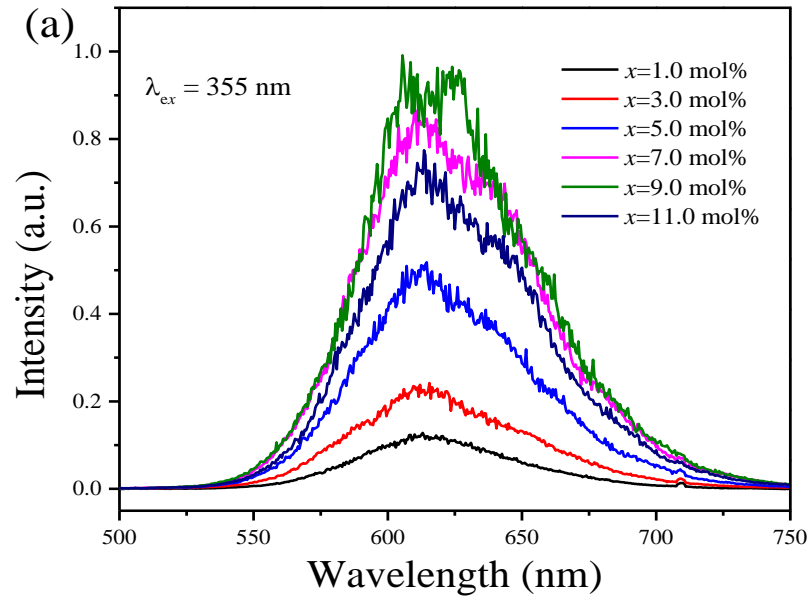
Then, the Mn^{2+} concentration dependent CIE values of the $\text{Na}_2\text{Mg}(\text{PO}_3)_4:\text{Mn}^{2+}$ phosphors were evaluated based on the Mn^{2+} concentration dependent PL spectra as presented in Figure. 4.3(a). According to the coordinates, the values of CP were calculated in the region of 85.7 to 88.4% as a function of Mn^{2+} ions in $\text{Na}_2\text{Mg}(\text{PO}_3)_4:\text{Mn}^{2+}$ phosphors. Particularly, the CCT value for prepared phosphors is calculated to lie in the range 1673 - 1788 K. The CIE values, color purity, and the chromaticity coordinate of the $\text{Na}_2\text{Mg}(\text{PO}_3)_4:\text{Mn}^{2+}$ phosphor were given in Table 4.1.

Figure. 4.3(c) shows luminescence decay curves of the ${}^4\text{T}_1$ emitting state in $\text{Na}_2\text{Mg}(\text{PO}_3)_4:\text{Mn}^{2+}$ phosphors for various Mn^{2+} concentration excited by 355 nm. In most of host crystals, the PL decay dynamics of Mn^{2+} ions is attributed to coexistence of emissions from isolated Mn^{2+} ions and $\text{Mn}^{2+}\text{-Mn}^{2+}$ pairs or clusters, which shows slow and fast PL decay time, respectively [90]. Therefore, the experimental data can be fitted by a single exponential decay function for the sample doping with low Mn^{2+} ions concentration and show multi-exponential decay curves for the sample doping with high Mn^{2+} ions concentration, as the red lines shown in Figure. 4.3(d). All the effective lifetimes were calculated based on the decay curves as the following equation:

$$\tau_{\text{avg}} = \frac{\int tI(t)dt}{\int I(t)dt} \quad (4.4)$$

where $I(t)$ represents the PL intensity at time t after the excitation light is cut off. As previously revealed, all decay lifetimes at millisecond scale are due to the properties of 3d shells in Mn^{2+} ions. The evaluated experimental lifetimes (τ) are listed in Table 4.2, which are comparable to that of Mn doped $\beta-Zn_2SiO_4$ (13-18 ms). In addition, the lifetimes of the 4T_1 emitting state in $Na_2Mg(PO_3)_4:Mn^{2+}$ phosphors gradually decreased from 23.97 to 22.81 ms with increasing the doping concentration of Mn^{2+} ions, which could give rise to a high radiative energy transfer rates ($A_{rad} = 1/\tau$) in the region from 0.0417 to 0.0438 ms^{-1} , thus produces a high intensity emission at 613 nm of Mn^{2+} ions. Meanwhile, the reason for the monotonously decline of lifetimes can be ascribed to the increasing possibility of nonradiative energy migration among Mn^{2+} ions [92].





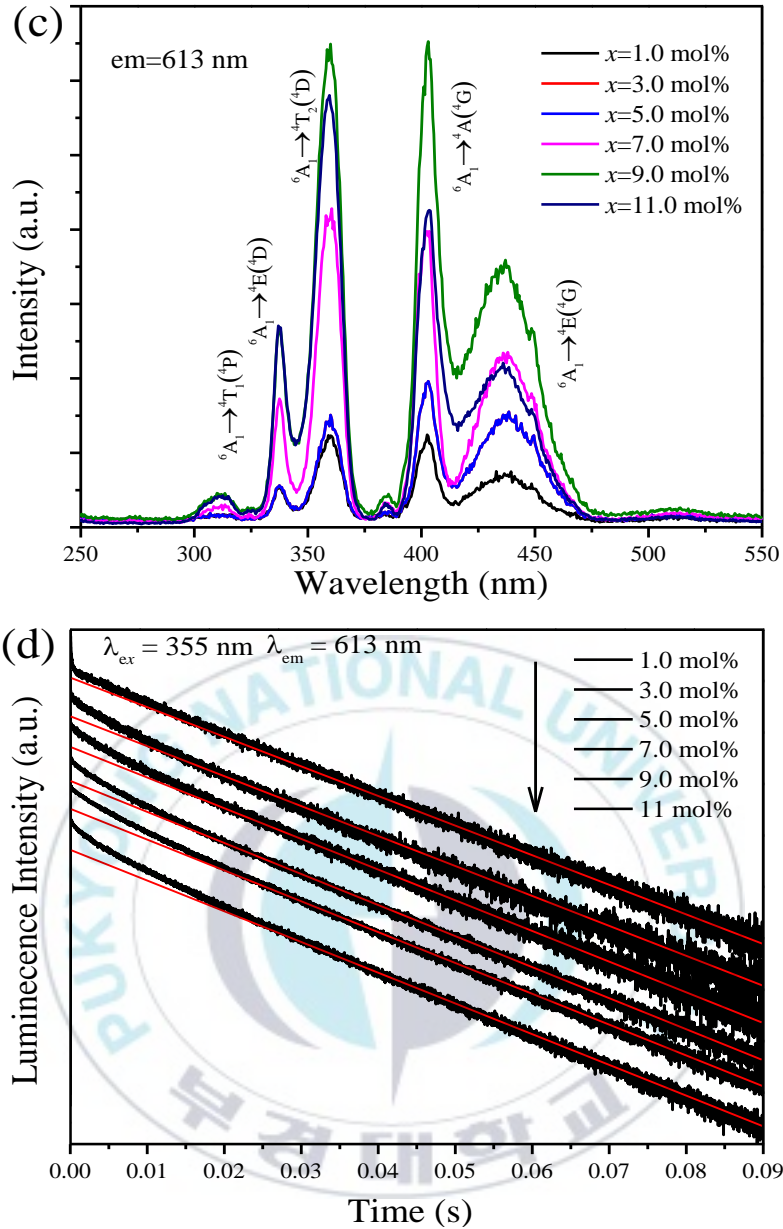
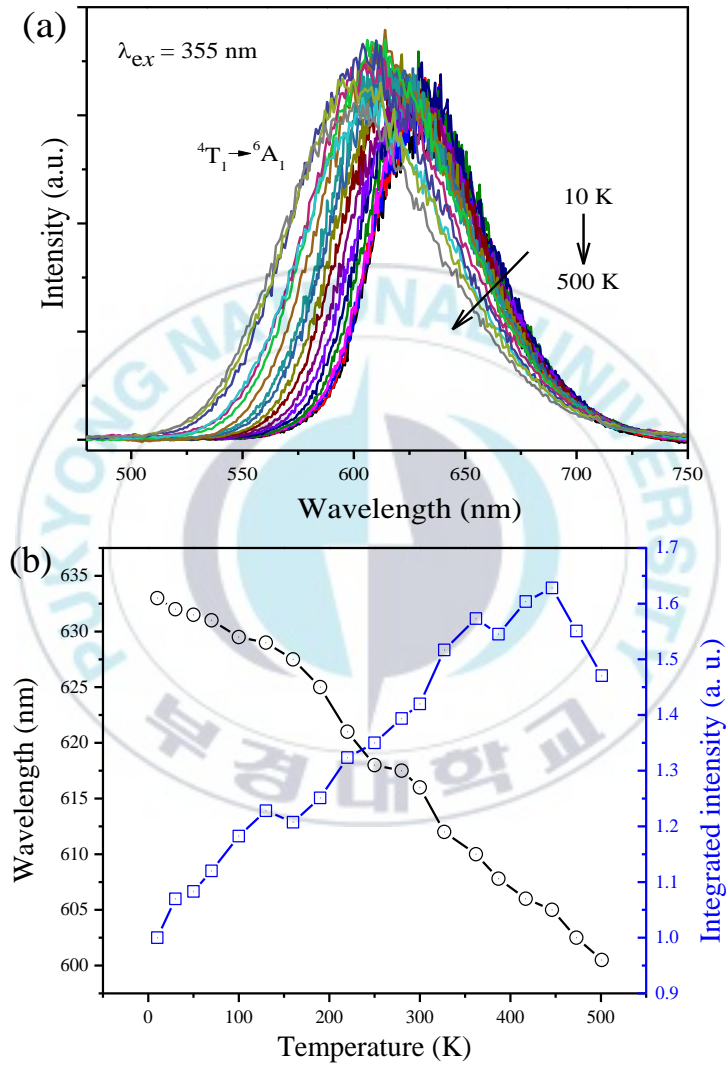


Figure 4.3. (a) Luminescence emission spectra ($\lambda_{\text{ex}} = 355 \text{ nm}$) of phosphors $\text{Na}_2\text{Mg}_{1-x}(\text{PO}_3)_4:x\text{Mn}^{2+}$ with different Mn^{2+} doping concentration. (b) The integrated PL intensity versus the concentration of Mn^{4+} ions; insert shows the $\text{Log}(1/x)$ dependent on $\text{Log}(x)$. (c) Luminescence excitation spectra ($\lambda_{\text{em}} = 613 \text{ nm}$) of phosphors $\text{Na}_2\text{Mg}_{1-x}(\text{PO}_3)_4:x\text{Mn}^{2+}$ with different Mn^{2+} doping concentration. (d) The decay curves ($\lambda_{\text{ex}} = 355 \text{ nm}$) of phosphors $\text{Na}_2\text{Mg}_{1-x}(\text{PO}_3)_4:x\text{Mn}^{2+}$ with different Mn^{2+} doping concentration.

4.2.4 The temperature dependent luminescence properties in Mn^{2+} -doped $\text{Na}_2\text{Mg}(\text{PO}_3)_4$

Generally, since the junction temperature increases with the increase of current, the reduction of chromaticity drift and luminous efficiency are the key problems of white-LEDs, especially

for the high power ones, the thermal quenching behavior is an important technological parameter due to the considerable influence on the color rendering index and the light output. The mechanism of temperature influenced on the emission of Mn^{2+} ions is complicated and the PL spectra of $Na_2Mg(PO_3)_4:9\%Mn^{2+}$ excited by 355 nm at various temperatures were shown in Figure. 4.4a. There are some optical characteristics should be noted:



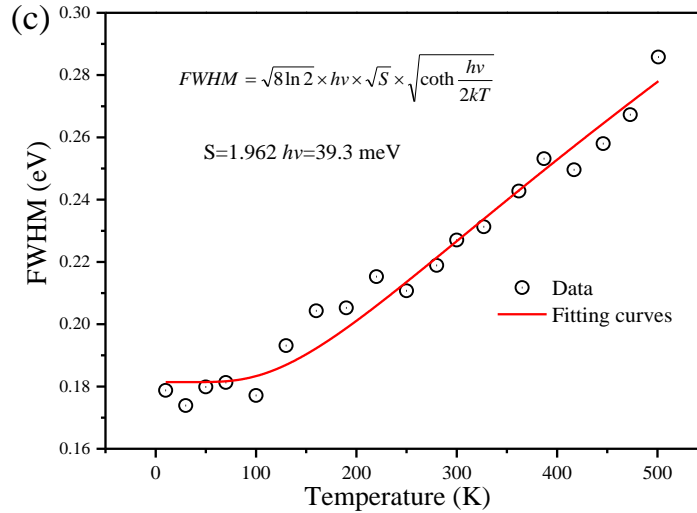


Figure 4.4. (a) Temperature-dependent emission spectra ($\lambda_{ex} = 355$ nm) of phosphors $\text{Na}_2\text{Mg}_{0.91}\text{Mn}_{0.09}(\text{PO}_3)_4$. (b) Temperature-dependent luminescence wavelength center and integrated luminescence intensities. (c) The variation in FWHM values from 10-500 K for $\text{Na}_2\text{Mg}_{0.91}\text{Mn}_{0.09}(\text{PO}_3)_4$ phosphor.

Firstly, as the temperature increases, the emission peak moves toward lower energies. As shown in Figure. 4.4a. the emission peak shifted significantly from 633 - 602 nm with the increase of temperature. In general, according to the Varshni equation, the emission wavelength should be shifted towards lower energy (redshift) as the temperature increases [84, 93, 94].

$$E(T) = E_0 - \frac{aT^2}{T + b} \quad (4.5)$$

where $E(T)$ represents the energy difference between the ground state and the excited state at temperature T , a and b represent the fitting parameters. The unusual properties suggest that some internal structure effects exert on the optical performance. However, until now, the detailed crystal structure of $\text{Na}_2\text{Mg}(\text{PO}_3)_4$ is not clear. Here, according to the reference, a tentative luminescence mechanism was proposed. The unusual properties can be explained by thermally active phonon assisted excitation from low energy level to high energy level. That is to say, at low temperature, the systems are more likely to be distributed in the vibrational ground state, where only relaxation back to ground with zero-phonon lines (ZPL) and Stokes emission primarily occurs. However, as the temperature rises, the electrons have enough energy to populate the upper vibration state and relax back to ground state with anti-Stokes emission. Consequently, the emission wavelength Mn^{2+} presents blue shift behavior. But, quite apart from

that, it could also be explained by the expansion of the host lattice with increasing temperature, which results in a reduction in the crystal field splitting and leads to higher emission energies.

The luminescence intensity increases firstly and then decreases due to the thermal quenching behavior. Figure. 4.4b shows the temperature dependent integrated emission intensity of Mn^{2+} ions normalized with respect to the value at 10 K. With increasing the temperature from 10 K to 500 K, the emission intensity increased to 165% (450 K) of the initial value (10 K), and then decreased to 146 % at 500 K. Usually, the emission intensities always decreased with temperature increase, which can be explained by thermal quenching behavior through the configurational coordinate (CC) model as shown in Figure. 4.5. Here, in this work, the increased emission intensity also can be attribute to phonon-assisted excitation from low energy level to high energy level as mentioned above. Overall, it clearly demonstrates that $\text{Na}_2\text{Mg}(\text{PO}_3)_4:\text{Mn}^{2+}$ phosphor shows excellent thermal stability [34, 95].

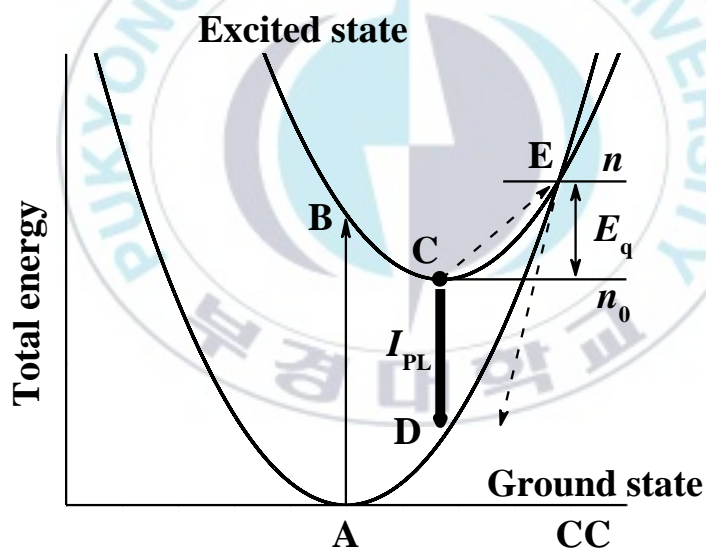


Figure 4.5. The schematic diagram of CC model used to explain the various intra-d-transition phenomena.

The emission band widens as the temperature increases. For phosphors, an increase in temperature can produce more thermally active phonons, which can help electrons to jump from the low energy excited states to the high energy excited states. In Figure. 4.4c, the full width at half maximum (FWHM) of $\text{Na}_2\text{Mg}(\text{PO}_3)_4:\text{Mn}^{2+}$ emission continues to increase with increasing temperature. As the excited electrons diffuse to high vibrational energy levels at high

temperature, the radiative transitions from these energy levels give rise to the broadening of the emission band with the increase of temperature. The variation of the FWHM values along with temperature can be described by the following equation based on the configuration coordinate model and Boltzmann distribution:

$$\text{FWHM} = \sqrt{8 \ln 2} \times hv \times \sqrt{S} \times \sqrt{\coth\left(\frac{hv}{2kT}\right)} \quad (4.6)$$

where S represents Huang-Rhys parameter, hv represents vibrational phonon energy, and k represents the Boltzmann constant. The best fitting value can be obtained with $S = 1.962$ and $hv = 39.3$ meV. The Huang-Rhys factor reveals the weak electron phonon interaction in $\text{Na}_2\text{Mg}(\text{PO}_3)_4:\text{Mn}^{2+}$ and also provides evidence for the good thermal photo-luminescence properties of $\text{Na}_2\text{Mg}(\text{PO}_3)_4:\text{Mn}^{2+}$.

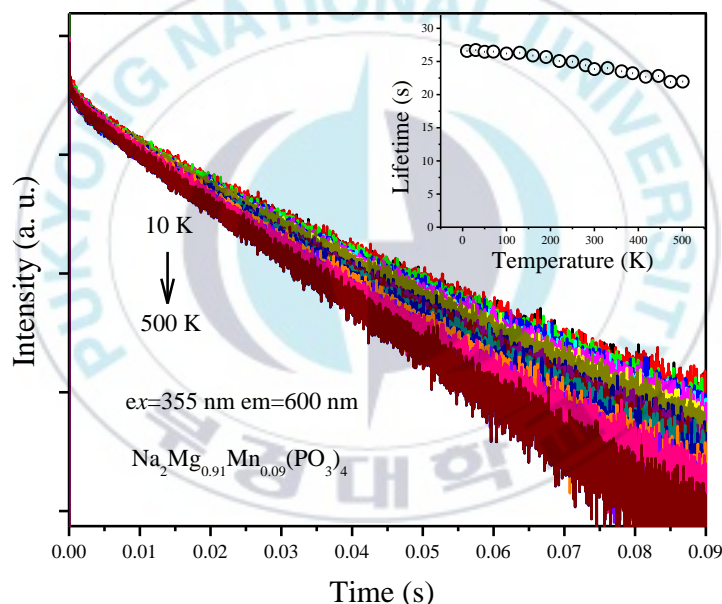


Figure 4.6. Temperature-dependent decay curves ($\lambda_{\text{ex}} = 355$ nm) of phosphors $\text{Na}_2\text{Mg}_{0.91}\text{Mn}_{0.09}(\text{PO}_3)_4$ monitored by 613 nm. Insert shows the calculated temperature-dependent luminescence lifetimes of the Mn^{2+} ions in $\text{Na}_2\text{Mg}_{0.91}\text{Mn}_{0.09}(\text{PO}_3)_4$ lattice.

According to the CC model as mentioned above, the temperature dependent decay curves were introduced as shown in Figure. 4.6. It can be seen that the luminescence remains stable in the region from 10 to 100 K, and when the temperature exceeds 100 K, the luminescence decreases slightly. The lifetimes can be calculated as a function of temperature and are listed in the insert of Figure. 4.6. The obtained results indicate that the lifetimes are not significantly

affected by temperatures in the region from 10 to 500 K. The lifetime retains several milliseconds with the longest lifetime of 26.58 ms and the shortest lifetime of 21.97 ms. Usually, due to thermal quenching behavior effects, for example thermally activated photoionization from excited state to conduction band, thermally activated nonradiative transition or multiphonon relaxation, the lifetimes of some phosphor decrease with the increase of temperature. However, the $\text{Na}_2\text{Mg}(\text{PO}_3)_4:0.09\text{Mn}^{2+}$ phosphor shows excellent thermal stability with low thermal quenching effects, especially in the low temperature range. Such unusual property also has been reported in some other Mn^{2+} doped materials, for example the $\text{Mn}:\text{ZnS}$ quantum dots with thick shells exhibit high quenching temperature of more than 200 °C.

The thermal activation energy (ΔE) was introduced to evaluate the thermal quenching behavior of the Mn^{2+} ions in $\text{Na}_2\text{Mg}(\text{PO}_3)_4$ lattice, which can be determined by the temperature dependent lifetimes of the Mn^{2+} ions as shown in:

$$\tau(T) = \frac{\tau r}{1 + \left[\frac{\tau r}{\tau_{nr}}\right] \exp\left(-\frac{\Delta E}{kT}\right)} \quad (4.6)$$

where τ_r and τ_{nr} represent the radiative and non-radiative lifetimes at temperature T, respectively, and k represents the Boltzmann constant. The ΔE fits to 0.3678 eV, which is comparable to that of other Mn^{2+} -doped luminescent materials, such as, $\text{Zn}_2\text{GeO}_4:\text{Mn}^{2+}$ with 0.36 eV. The unusual thermal stability indicates that Mn^{2+} doped materials have unique properties and potential applications.

4.3 Conclusions

In summary, $\text{Na}_2\text{Mg}_{1-x}(\text{PO}_3)_4:x\text{Mn}^{2+}$ red phosphors with various doping concentration of Mn^{2+} ions were synthesized by solid-state method and the crystal structure were determined by XRD measurement. The overall luminescence performances were evaluated through PL spectra, PLE spectra, and decay curves. $\text{Na}_2\text{Mg}(\text{PO}_3)_4:\text{Mn}^{2+}$ red phosphor exhibits strong and broad absorption ranging from 300 to 500 nm and exhibits bright red emission at 613 nm, which can be attributed to the ${}^4\text{T}_1 \rightarrow {}^6\text{A}_1$ transition of Mn^{2+} ions. Temperature dependence of luminescence indicates that $\text{Na}_2\text{Mg}(\text{PO}_3)_4:\text{Mn}^{2+}$ red phosphor shows excellent thermal stability, and the

thermal quenching temperature is higher than 450 K. With the increase in temperature, the emission wavelength Mn^{2+} ions are slightly blue shifted and the emission spectrum becomes broaden, which can be explained by the transition of thermally active phonon-assisted excitation from low energy level to high energy level in Mn^{2+} ions. The ΔE was calculated to be 0.3678 eV, which is comparable to that of other Mn^{2+} -doped luminescent materials. All results indicate that the $\text{Na}_2\text{Mg}(\text{PO}_3)_4:\text{Mn}^{2+}$ red phosphor is a good non rare earth ions doped red-emitting phosphor for use in white-light LEDs.



References

- [1] J.V. Vleck, The Puzzle of Rare-earth Spectra in Solids, *Journal of physical chemistry*, 41 (1937) 67-80.
- [2] J. Blochwitz, M. Pfeiffer, T. Fritz, K. Leo, Low voltage organic light emitting diodes featuring doped phthalocyanine as hole transport material, *Applied Physics Letters*, 73 (1998) 729-731.
- [3] Z. Xu, S. Bian, T. Liu, L. Wang, Y. Gao, H. Lian, J. Lin, Self-assembled growth of LuVO₄ nanoleaves: hydrothermal synthesis, morphology evolution, and luminescence properties, *RSC Advances*, 2 (2012) 11067.
- [4] J. Feng, L. Xiong, S. Wang, S. Li, Y. Li, G. Yang, Fluorescent Temperature Sensing Using Triarylboron Compounds and Microcapsules for Detection of a Wide Temperature Range on the Micro-and Macroscale, *Advanced Functional Materials*, 23 (2013) 340-345.
- [5] L. Qin, D. Wei, Y. Huang, S.I. Kim, Y.M. Yu, H.J. Seo, Triple-Layered Perovskite Niobates CaRNb₃O₁₀ (R= La, Sm, Eu, Gd, Dy, Er, Yb, or Y): New Self-Activated Oxides, *Inorganic chemistry*, 52 (2013) 10407-10413.
- [6] G. Blasse, B. Grabmaier, How does a luminescent material absorb its excitation energy?, in: *Luminescent materials*, Springer, 1994, pp. 10-32.
- [7] K. Shinde, S. Dhoble, Europium-activated orthophosphate phosphors for energy-efficient solid-state lighting: a review, *Critical Reviews in Solid State and Materials Sciences*, 39 (2014) 459-479.
- [8] N. Holonyak Jr, S.F. Bevacqua, Coherent (visible) light emission from Ga (As_{1-x}P_x) junctions, *Applied Physics Letters*, 1 (1962) 82-83.
- [9] Z. Qiao, X. Wang, C. Heng, W. Jin, L. Ning, Exploring Intrinsic Electron-Trapping Centers for Persistent Luminescence in Bi³⁺-Doped LiREGeO₄ (RE = Y, Sc, Lu): Mechanistic Origin from First-Principles Calculations, *Inorganic chemistry*, 60 (2021) 16604-16613.
- [10] Y. Hasegawa, K. Murakoshi, Y. Wada, S. Yanagida, J.-H. Kim, N. Nakashima, T. Yamanaka, Enhancement of luminescence of Nd³⁺ complexes with deuterated hexafluoroacetylacetonato ligands in organic solvent, *Chemical physics letters*, 248 (1996) 8-12.
- [11] N. Bloembergen, Solid state infrared quantum counters, *Physical Review Letters*, 2 (1959) 84.
- [12] K.P. Mani, G. Vimal, P. Biju, N. Unnikrishnan, M. Ittyachen, C. Joseph, Synthesis and optical characterization of host sensitized color tunable Tb_{2-x}Eu_x(MoO₄)₃ nanophosphors for optoelectronic applications, *Journal of Materials Science: Materials in Electronics*, 27 (2016) 966-975.
- [13] E.M. Goldys, K. Drozdowicz-Tomsia, S. Jinjun, D. Dosev, I.M. Kennedy, S. Yatsunenko, M. Godlewski, Optical characterization of Eu-doped and undoped Gd₂O₃ nanoparticles synthesized by the hydrogen flame pyrolysis method, *Journal of the American Chemical Society*, 128 (2006) 14498-14505.
- [14] X. Xurong, S. Mianzeng, L. Hongkai, Luminescence and luminescent materials [M], in, Beijing: Chemical Industry Press, 2004.
- [15] L. Liu, Q. Wang, C. Gao, H. Chen, W. Liu, Y. Tang, Dramatically enhanced luminescence of layered terbium hydroxides as induced by the synergistic effect of Gd³⁺ and organic sensitizers, *The Journal of Physical Chemistry C*, 118 (2014) 14511-14520.
- [16] J.W. Stouwdam, G.A. Hebbink, J. Huskens, F.C. van Veggel, Lanthanide-doped nanoparticles with excellent luminescent properties in organic media, *Chemistry of Materials*, 15 (2003) 4604-4616.
- [17] X. Qi, Z. Sui, Y. Deng, R. Dai, Z. Wang, Z. Zhang, Z. Ding, Pressure and temperature dependent

- up-conversion properties of Yb³⁺-Er³⁺ co-doped BaBi₄Ti₄O₁₅ ferroelectric ceramics, *Journal of Rare Earths*, 32 (2014) 879-883.
- [18] S.V. Eliseeva, J.-C.G. Bünzli, Lanthanide luminescence for functional materials and bio-sciences, *Chemical Society Reviews*, 39 (2010) 189-227.
- [19] H. Guo, H. Qian, N.M. Idris, Y. Zhang, Singlet oxygen-induced apoptosis of cancer cells using upconversion fluorescent nanoparticles as a carrier of photosensitizer, *Nanomedicine: Nanotechnology, Biology and Medicine*, 6 (2010) 486-495.
- [20] L.D. Carlos, R.A. Ferreira, V.d.Z. Bermudez, S.J. Ribeiro, Lanthanide-containing light-emitting organic-inorganic hybrids: a bet on the future, *Advanced Materials*, 21 (2009) 509-534.
- [21] A. Vink, M. De Bruin, S. Roke, P. Peijzel, A. Meijerink, Luminescence of exchange coupled pairs of transition metal ions, *Journal of The Electrochemical Society*, 148 (2001) E313-E320.
- [22] L. Qin, P. Cai, C. Chen, J. Wang, S.I. Kim, Y. Huang, H.J. Seo, Optical performance of the Ba₅Al₃F₁₉:Eu²⁺ blue phosphors with high thermal stability, *Journal of Alloys and Compounds*, 738 (2018) 372-378.
- [23] C. Cao, X. Yang, X. Chen, A. Xie, Enhanced emission of Eu³⁺ in lutetium tungsten molybdenum oxide phosphors: Synthesis, optical properties, thermal behavior, and LED packaging, *Journal of Luminescence*, 223 (2020) 117269.
- [24] H. Cheng, L. Qin, P. Cai, C. Chen, J. Wang, S.I. Kim, Y. Huang, H.J. Seo, Charge transfer transition and energy transfer in Eu³⁺-doped Gd₁₀V₂O₂₀, *Journal of Luminescence*, 195 (2018) 278-282.
- [25] H. Guo, X. Huang, Y. Zeng, Synthesis and photoluminescence properties of novel highly thermal-stable red-emitting Na₃Sc₂(PO₄)₃:Eu³⁺ phosphors for UV-excited white-light-emitting diodes, *Journal of Alloys and Compounds*, 741 (2018) 300-306.
- [26] J. Liang, L. Sun, G. Annadurai, B. Devakumar, S. Wang, Q. Sun, J. Qiao, H. Guo, B. Li, X. Huang, Synthesis and photoluminescence characteristics of high color purity Ba₃Y₄O₉:Eu³⁺ red-emitting phosphors with excellent thermal stability for warm W-LED application, *RSC Advances*, 8 (2018) 32111-32118.
- [27] C.h.B. Annapurna Devi, S. Mahamuda, K. Swapna, M. Venkateswarlu, A. Srinivasa Rao, G. Vijaya Prakash, Compositional dependence of red luminescence from Eu³⁺ ions doped single and mixed alkali fluoro tungsten tellurite glasses, *Optical Materials*, 73 (2017) 260-267.
- [28] F. Liang, Y.-H. Hu, L. Chen, X.-J. Wang, Energy transfer between WO₄²⁻ groups and Eu³⁺ in CaWO₄:Eu³⁺ phosphor, *Acta Physica Sinica*, 62 (2013) 183302.
- [29] T. Zheng, M. Runowski, P. Woźny, S. Lis, Influence of matrix on the luminescence properties of Eu²⁺/Eu³⁺ doped strontium borates: SrB₄O₇, SrB₂O₄ and Sr₃(BO₃)₂, exhibiting multicolor tunable emission, *Journal of Alloys and Compounds*, 822 (2020) 153511.
- [30] P. Du, X. Huang, J.S. Yu, Facile synthesis of bifunctional Eu³⁺-activated NaBiF₄ red-emitting nanoparticles for simultaneous white light-emitting diodes and field emission displays, *Chemical Engineering Journal*, 337 (2018) 91-100.
- [31] Q. Ma, Y. Zhou, M. Lu, A. Zhang, G. Zhou, Synthesis and luminescence of pure and Eu³⁺-activated Aurivillius-type Bi₃TiNbO₉ nanophosphors, *Materials Chemistry and Physics*, 116 (2009) 315-318.
- [32] P. Cai, S. Wang, T. Xu, Y. Tang, X. Yuan, M. Wan, Q. Ai, J. Si, X. Yao, Y. Cao, M.K. Rabchinskii, P.N. Brunkov, Z. Liu, Mn⁴⁺ doped zero-dimensional organic-inorganic hybrid material with narrow-red emission, *Journal of Luminescence*, 228 (2020) 117661.
- [33] R. Laishram, R. Gaur, K.C. Singh, C. Prakash, Control of coring effect in BaTiO microwave dielectric ceramics by doping with Mn⁴⁺, *Ceramics International*, 42 (2016) 5286-5290.

- [34] C.H. Huang, T.W. Kuo, T.M. Chen, Novel red-emitting phosphor $\text{Ca}_9\text{Y}(\text{PO}_4)_7:\text{Ce}^{3+},\text{Mn}^{2+}$ with energy transfer for fluorescent lamp application, *ACS applied materials & interfaces*, 2 (2010) 1395-1399.
- [35] Y. Tanabe, S. Sugano, On the absorption spectra of complex ions II, *Journal of the Physical Society of Japan*, 9 (1954) 766-779.
- [36] Y. Tanabe, S. Sugano, On the absorption spectra of complex ions, III The calculation of the crystalline field strength, *Journal of the Physical Society of Japan*, 11 (1956) 864-877.
- [37] J.-Y. Li, D. Hou, Y. Zhang, H. Li, H. Lin, Z. Lin, W. Zhou, R. Huang, Luminescence, energy transfer and temperature sensing property of Ce^{3+} , Dy^{3+} doped $\text{LiY}_9(\text{SiO}_4)_6\text{O}_2$ phosphors, *Journal of Luminescence*, 213 (2019) 184-190.
- [38] R. Vijayakumar, B. Devakumar, X. Huang, Energy transfer induced color-tunable emissions from $\text{Ba}_2\text{Gd}_5\text{B}_5\text{O}_{17}:\text{Ce}^{3+}/\text{Tb}^{3+}$ borate phosphors for white LEDs, *Journal of Luminescence*, 229 (2021) 117685.
- [39] T.H.Q. Vu, B. Bondzior, D. Stefanska, P.J. Deren, Exploration of the Temperature Sensing Ability of $\text{La}_2\text{MgTiO}_6:\text{Er}^{3+}$ Double Perovskites Using Thermally Coupled and Uncoupled Energy Levels, *Materials*, 14 (2021).
- [40] H. Zhang, Y. Liang, H. Yang, S. Liu, H. Li, Y. Gong, Y. Chen, G. Li, Highly Sensitive Dual-Mode Optical Thermometry in Double-Perovskite Oxides via $\text{Pr}^{3+}/\text{Dy}^{3+}$ Energy Transfer, *Inorganic chemistry*, 59 (2020) 14337-14346.
- [41] F. Kish, F. Steranka, D. DeFevere, D. Vanderwater, K. Park, C. Kuo, T. Osentowski, M. Peanasky, J. Yu, R. Fletcher, Very high-efficiency semiconductor wafer-bonded transparent-substrate $(\text{Al}_x\text{Ga}_{1-x})_{0.5}\text{In}_{0.5}\text{P}/\text{GaP}$ light-emitting diodes, *Applied Physics Letters*, 64 (1994) 2839-2841.
- [42] K. Werner, Higher visibility for LEDs, *IEEE spectrum*, 31 (1994) 30-34.
- [43] H. Sugawara, K. Itaya, H. Nozaki, G. Hatakoshi, High-brightness InGaAlP green light-emitting diodes, *Applied physics letters*, 61 (1992) 1775-1777.
- [44] Z. Chen, B. Wang, X. Li, L. Kang, Y. Chen, Y. Chen, H. Sun, Q. Zeng, Facile synthesis of self-activated oxyfluorotungstate phosphor with high QE and its thermal quenching, *Journal of Alloys and Compounds*, 770 (2019) 559-563.
- [45] D. Zhao, J. Zhao, Y.-C. Fan, Z. Ma, R.-J. Zhang, B.-Z. Liu, Synthesis, crystal structure and luminescent properties of a new pyrochlore type tungstate $\text{CsGa}_{0.333}\text{W}_{1.667}\text{O}_6$, *Physica B: Condensed Matter*, 539 (2018) 97-100.
- [46] M. Zhang, Z. Lian, Y. Wang, S. Pan, Nonlinear optical and self-activated luminescent properties of $\text{A}_2\text{W}_3\text{O}_{10}$ (A= Rb and Cs), *RSC advances*, 6 (2016) 39234-39239.
- [47] Z. Feng, B. Lou, Q. Chen, M. Yin, C.G. Ma, C.K. Duan, Self-Activated and Bismuth-Related Photoluminescence in Rare-Earth Vanadate, Niobate, and Tantalate Series-A First-Principles Study, *Inorganic chemistry*, 60 (2021) 16614-16625.
- [48] D. Abeysinghe, M.D. Smith, J. Yeon, T.T. Tran, R. Paria Sena, J. Hadermann, P.S. Halasyamani, H.C. Zur Loye, Crystal Growth and Structure Analysis of $\text{Ce}_{18}\text{W}_{10}\text{O}_{57}$: A Complex Oxide Containing Tungsten in an Unusual Trigonal Prismatic Coordination Environment, *Inorganic chemistry*, 56 (2017) 2566-2575.
- [49] J. Czajka, A. Szczeszak, N. Kaczorowska, S. Lis, New Multicolor Tungstate-Molybdate Microphosphors as an Alternative to LED Components, *Materials*, 14 (2021).
- [50] M. Ding, D. Chen, C. Lu, J. Xi, Z. Ji, Z. Xu, Lanthanide-doped LuF_3 mesocrystals for optical thermometry, *Materials Letters*, 189 (2017) 5-8.

- [51] P. Du, L. Luo, J.S. Yu, Controlled synthesis and upconversion luminescence of Tm₃₊-doped NaYbF₄ nanoparticles for non-invasion optical thermometry, *Journal of Alloys and Compounds*, 739 (2018) 926-933.
- [52] V. Lojpur, S. Čulubrk, M. Medić, M. Dramicanin, Luminescence thermometry with Eu³⁺ doped GdAlO₃, *Journal of Luminescence*, 170 (2016) 467-471.
- [53] Z. Zikmund, The crystal structure of Ca₃WO₆Cl₂ and the configuration of the WO₅⁴⁻ ion, *Acta Crystallographica Section B: Structural Crystallography and Crystal Chemistry*, 30 (1974) 2587-2593.
- [54] D. Hirai, T. Yajima, K. Nawa, M. Kawamura, Z. Hiroi, Anisotropic Triangular Lattice Realized in Rhenium Oxychlorides A₃ReO₅Cl₂ (A= Ba, Sr), *Inorganic chemistry*, 59 (2020) 10025-10033.
- [55] M. Hazenkamp, E. Voogt, G. Blasse, Luminescence of two dioxido transition-metal complexes: K₂MoO₂F₄· H₂O and NaWO₂PO₄, *Journal of Solid State Chemistry*, 101 (1992) 26-31.
- [56] G. Blasse, G. Bokkers, Low-temperature decay-time measurements on the luminescence of calcium tungstate (CaWO₄), *Journal of Solid State Chemistry*, 49 (1983) 126-128.
- [57] M. Lammers, G. Blasse, Luminescence of sodium molybdate (Na₂Mo₂O₇) and sodium tungstate (Na₂W₂O₇), *physica status solidi (a)*, 63 (1981) 157-161.
- [58] G. Blasse, H. Verhaar, M. Lammers, G. Wingefeld, R. Hoppe, P. De Maayer, Ba₂WO₃F₄, a new fluorotungstate with high luminescence efficiency, *Journal of luminescence*, 29 (1984) 497-499.
- [59] E. Mihokova, M. Nikl, P. Bohacek, V. Babin, A. Krasnikov, A. Stolovich, S. Zazubovich, A. Vedda, M. Martini, T. Grabowski, Decay kinetics of the green emission in PbWO₄: Mo, *Journal of luminescence*, 102 (2003) 618-622.
- [60] A. Srivastava, J. Ackerman, Structure and luminescence of Cs₂WO₂F₄: Efficient luminescence of isolated [WO₂F₄]⁻² octahedra, *Journal of Solid State Chemistry*, 98 (1992) 144-150.
- [61] X. Chen, T. Zhao, L. Qin, The red-emitting phosphors of Mn⁴⁺-activated A₂MgWO₆ (A= Ba, Sr, Ca) for light emitting diodes, *Ceramics International*, 47 (2021) 6010-6022.
- [62] W. Van Loo, Luminescence decay of lead molybdate and lead tungstate—A descriptive model, *Journal of Luminescence*, 10 (1975) 221-235.
- [63] Y. Ohkubo, T. Saito, Y. Murakami, A. YOKOYAMA, Y. KAWASE, *Acta Crystallogr., Sect. A: Cryst. Phys., Diffr., Theor. Gen. Crystallogr. Acta Crystallogr., Sect. A: Cryst. Phys., Diffr., Theor. Gen. Crystallogr.* 32, 751-767, 1976, *Materials transactions*, 43 (2002) 1469-1474.
- [64] P. Paulose, G. Jose, V. Thomas, N. Unnikrishnan, M. Warriar, Sensitized fluorescence of Ce³⁺/Mn²⁺ system in phosphate glass, *Journal of Physics and Chemistry of Solids*, 64 (2003) 841-846.
- [65] D.L. Dexter, J.H. Schulman, Theory of concentration quenching in inorganic phosphors, *The Journal of chemical physics*, 22 (1954) 1063-1070.
- [66] R. Reisfeld, E. Greenberg, R. Velapoldi, B. Barnett, Luminescence quantum efficiency of Gd and Tb in borate glasses and the mechanism of energy transfer between them, *The Journal of chemical physics*, 56 (1972) 1698-1705.
- [67] X. Zhang, Z. Zhang, S.I. Kim, Y. Moon Yu, H.J. Seo, Photoluminescence properties of Eu³⁺ in garnet-type Li₇La₃Zr₂O₁₂ polycrystalline ceramics, *Ceramics International*, 40 (2014) 2173-2178.
- [68] A. Setlur, H. Comanzo, A. Srivastava, W. Beers, Spectroscopic evaluation of a white light phosphor for UV-LEDs—Ca₂NaMg₂V₃O₁₂: Eu³⁺, *Journal of the Electrochemical Society*, 152 (2005) H205.
- [69] G. Blasse, A. Bril, Fluorescence of Eu³⁺-Activated Garnets Containing Pentavalent Vanadium, *Journal of the Electrochemical Society*, 114 (1967) 250.
- [70] C. Hsu, R.C. Powell, Energy transfer in europium doped yttrium vanadate crystals, *Journal of*

- Luminescence, 10 (1975) 273-293.
- [71] L. Qin, D.-L. Wei, Y. Huang, C. Qin, P. Cai, S.-I. Kim, H.-J. Seo, Ortho-vanadates $K_3RE(VO_4)_2$ (RE= La, Pr, Eu, Gd, Dy, Y) for near UV-converted phosphors, *Materials Chemistry and Physics*, 147 (2014) 1195-1203.
- [72] F. Meng, X. Zhang, Y.M. Yu, S.I. Kim, H.J. Seo, Synthesis and luminescence properties of a $La_2W_3O_{12}:Eu^{3+}$ phosphor for near-UV white LEDs, *Journal of the Korean Physical Society*, 64 (2014) 104-108.
- [73] X. Zhang, H.J. Seo, Color tunable and thermally stable luminescence of Tb^{3+} doped $Li_4SrCa(SiO_4)_2$ phosphors, *Materials Research Bulletin*, 47 (2012) 2012-2015.
- [74] L. Qin, D. Wei, Y. Huang, S.I. Kim, Y.M. Yu, H.J. Seo, Triple-layered perovskite niobates $CaRNb_3O_{10}$ (R = La, Sm, Eu, Gd, Dy, Er, Yb, or Y): new self-activated oxides, *Inorganic chemistry*, 52 (2013) 10407-10413.
- [75] G. Dong, J. Zhao, M. Li, L. Guan, X. Li, A novel red $Y_2MoSiO_8: Eu^{3+}$ phosphor with high thermal stability for white LEDs, *Ceramics International*, 45 (2019) 2653-2656.
- [76] L. Zhang, Y. Xie, X. Geng, B. Deng, H. Geng, R. Yu, Double perovskite $Ca_2MgTeO_6: Eu^{3+}$ red-emitting phosphors with high thermal stability for near UV/blue excited white LEDs, *Journal of Luminescence*, 225 (2020) 117365.
- [77] L. Zhang, B. Deng, S. Shu, Y. Wang, H. Geng, R. Yu, Preparation, characterization, and luminescence properties of $BiLaWO_6: Eu^{3+}$ red-emitting phosphors for w-LEDs, *Spectrochimica Acta Part A: Molecular and Biomolecular Spectroscopy*, 224 (2020) 117454.
- [78] Y. Huang, H.J. Seo, Multisite structure of $PbWO_4:Eu^{3+}$ crystals investigated by site-selective laser-excitation spectroscopy, *The journal of physical chemistry. A*, 113 (2009) 5317-5323.
- [79] J. Xiao, C. Wang, X. Min, X. Wu, Y. Liu, Z. Huang, M. Fang, Multiple Energy Transfer in Luminescence-Tunable Single-Phased Phosphor $NaGdTiO_4: Tm^{3+}, Dy^{3+}, Sm^{3+}$, *Nanomaterials*, 10 (2020).
- [80] Y. Wang, Z. Lian, X. Su, Z. Yang, S. Pan, Q. Yan, F. Zhang, $Cs_6RE_2(PO_4)_4$ (RE = Y and Gd): two new members of the alkali rare-earth double phosphates, *New Journal of Chemistry*, 39 (2015) 4328-4333.
- [81] Y. Li, J. Wang, Y. Huang, H.J. Seo, Temperature-Dependent $^5D_0 \rightarrow ^7F_0$ Luminescence of Sm^{2+} Ions Doped in Alkaline Earth Borophosphate Glass, *Journal of the American Ceramic Society*, 93 (2010) 722-726.
- [82] C. Poesl, W. Schnick, $Ca_4Mg_5Ge_3N_{10}$ and $Sr_2Mg_3GaN_{4.33}$: Two Mg-Containing Nitrides and Their Structural Relation to $(Sr, Ba)_2Si_5N_8$, *European Journal of Inorganic Chemistry*, 2017 (2017) 1498-1503.
- [83] Y. Shi, Y. Wen, M. Que, G. Zhu, Y. Wang, Structure, photoluminescent and cathodoluminescent properties of a rare-earth free red emitting $\beta-Zn_3B_2O_6: Mn^{2+}$ phosphor, *Dalton transactions*, 43 (2014) 2418-2423.
- [84] Z. Zhang, C. Ma, R. Gautier, M.S. Molokeev, Q. Liu, Z. Xia, Structural confinement toward giant enhancement of red emission in Mn^{2+} -based phosphors, *Advanced Functional Materials*, 28 (2018) 1804150.
- [85] H. You, J. Zhang, G. Hong, H. Zhang, Luminescent properties of Mn^{2+} in hexagonal aluminates under ultraviolet and vacuum ultraviolet excitation, *The Journal of Physical Chemistry C*, 111 (2007) 10657-10661.
- [86] J. Zhou, Y. Wang, B. Liu, Y. Lu, Effect of H_3BO_3 on structure and photoluminescence of $BaAl_{12}O_{19}$:

- Mn²⁺ phosphor under VUV excitation, *Journal of Alloys and Compounds*, 484 (2009) 439-443.
- [87] C. Duan, A. Delsing, H. Hintzen, Photoluminescence properties of novel red-emitting Mn²⁺-activated MZnOS (M= Ca, Ba) phosphors, *Chemistry of Materials*, 21 (2009) 1010-1016.
- [88] Y. Liu, J. Zhang, B. Han, X. Wang, Z. Wang, C. Xue, G. Bian, D. Hu, R. Zhou, D.-S. Li, New insights into Mn–Mn coupling interaction-directed photoluminescence quenching mechanism in Mn²⁺-doped semiconductors, *Journal of the American Chemical Society*, 142 (2020) 6649-6660.
- [89] L. Gaofeng, D. Degang, L. Yinqun, W. Qian, H. Youjie, X. Shiqing, Luminescence properties of Mn²⁺ ions doped Lu₂CaMg₂Si₃O₁₂ garnet phosphors, *Journal of Rare Earths*, 30 (2012) 193-196.
- [90] N. Xie, J. Liu, Y. Huang, S.I. Kim, H.J. Seo, Tunable luminescence properties and efficient energy transfer in Eu²⁺, Mn²⁺ co-doped Ba₂MgP₄O₁₃, *Ceramics International*, 38 (2012) 1489-1495.
- [91] C. Barthou, J. Benoit, P. Benalloul, A. Morell, Mn²⁺ concentration effect on the optical properties of Zn₂SiO₄: Mn phosphors, *Journal of the Electrochemical Society*, 141 (1994) 524.
- [92] R. Mason, M. Clouter, R. Goulding, The luminescence decay-time of Mn²⁺ activated calcite, *Physics and chemistry of minerals*, 32 (2005) 451-459.
- [93] X.M. Zhang, W.L. Li, H.J. Seo, Luminescence and energy transfer in Eu²⁺, Mn²⁺ co-doped Li₄SrCa(SiO₄)₂ for white light-emitting-diodes, *Physics Letters A*, 373 (2009) 3486-3489.
- [94] J.S. Kim, A.K. Kwon, Y.H. Park, J.C. Choi, H.L. Park, G.C. Kim, Luminescent and thermal properties of full-color emitting X₃MgSi₂O₈:Eu²⁺, Mn²⁺ (X=Ba, Sr, Ca) phosphors for white LED, *Journal of Luminescence*, 122-123 (2007) 583-586.
- [95] L. Shi, Y. Huang, H.J. Seo, Emission red shift and unusual band narrowing of Mn²⁺ in NaCaPO₄ phosphor, *The Journal of Physical Chemistry A*, 114 (2010) 6927-6934.
- [96] X. Yuan, J. Zheng, R. Zeng, P. Jing, W. Ji, J. Zhao, W. Yang, H. Li, Thermal stability of Mn²⁺ ion luminescence in Mn-doped core-shell quantum dots, *Nanoscale*, 6 (2014) 300-307.
- [97] R. Beaulac, P.I. Archer, D.R. Gamelin, Luminescence in colloidal Mn²⁺-doped semiconductor nanocrystals, *Journal of solid state chemistry*, 181 (2008) 1582-1589.
- [98] Y. Lv, Y. Jin, H. Wu, D. Liu, G. Xiong, G. Ju, L. Chen, Y. Hu, An all-optical ratiometric thermometer based on reverse thermal response from interplay among diverse emission centers and traps with high-temperature sensitivity, *Industrial & Engineering Chemistry Research*, 58 (2019) 21242-21251.
- [99] S. Park, D.R. Rittman, C.L. Tracy, K.W. Chapman, F. Zhang, C. Park, S.N. Tkachev, E. O'Quinn, J. Shamblin, M. Lang, W.L. Mao, R.C. Ewing, A₂TiO₅ (A = Dy, Gd, Er, Yb) at High Pressure, *Inorganic chemistry*, 57 (2018) 2269-2277.
- [100] J. Zhang, F. Zhang, L. Han, Investigation on luminescence of red-emitting Mg₃Ca₃(PO₄)₄:Ce³⁺, Mn²⁺ phosphors, *Journal of Rare Earths*, 33 (2015) 820-824.
- [101] Q. Bao, Z. Wang, J. Sun, Z. Wang, X. Meng, K. Qiu, Y. Chen, Z. Yang, P. Li, Crystal structure, luminescence properties, energy transfer, tunable occupation and thermal properties of a novel color-tunable phosphor NaBa_{1-z}Sr_zB₉O₁₅:xCe³⁺, yMn²⁺, *Dalton transactions*, 47 (2018) 13913-13925.
- [102] X. Zhang, H.J. Seo, Thermally stable luminescence and energy transfer in Ce³⁺, Mn²⁺ doped Sr₂Mg(BO₃)₂ phosphor, *Optical Materials*, 33 (2011) 1704-1709.

Acknowledgements

Time flies, PhD career is fleeting. Looking back at the past, I would like to thank all the teachers, relatives, and friends around me.

First, I would like to extend my sincere gratitude to my advisor Prof. Hyo Jin Seo. At the beginning of studying at Pukyong National University, I am very happy to be your student. The study is about to be completed; I am very grateful to be your student. Thank you for your help, support, encouragement, affirmation, and trust for me along the way. He has walked me through all the stages of the writing of this thesis. Without his consistent and illuminating instruction, this thesis could not have reached its present form.

I would like to appreciate to Prof. Yanlin Huang from Soochow University who gave me helps and let me into world of research work.

Thanks to my friends Zutao Fan, Donglei Wei, Jing Wang, Lin Qin, Peiqing Cai, Cuili Chen, et al. They often give me instructed and helped me a lot in the past five years.

At last, I'd like to dedicate this work to my family, especially my parents and my older brother. I have always been grateful, grateful that I can have such a warm family, they will always give me support and strength to do what I like. Thanks to all my relatives for their kind care and support.